Engineering Analysis with Boundary Elements 75 (2017) 21–35

Contents lists available at ScienceDirect

Engineering Analysis with Boundary Elements

journal homepage: www.elsevier.com/locate/enganabound

Evaluation of nearly singular integrals in isogeometric boundary element method

Y.P. Gong, C.Y. Dong*, Y. Bai

Department of Mechanics, School of Aerospace Engineering, Beijing Institute of Technology, Beijing 100081, China

ARTICLE INFO

Keywords:
2D/3D potential problems
IGBEM
Nearly singular integrals
Exponential transformation

ABSTRACT

Isogeometric boundary element method (IGBEM) is a new numerical method that has received a lot of attentions in recent years. However, nearly singular integrals in the IGBEM have not yet received more attention when the IGBEM is used to study thin-body/coating structures. In this paper, the exponential transformation method based on the idea of diminishing the difference of the orders or the scale of change of addition factors in the denominator of the kernels is used to remove or weaken the near singularities of nearly singular integrals appearing in 2D/3D potential problems. Numerical results show that the present method is effective, stable and competitive. We believe that this work clearly presents the power of the IGBEM and provides an efficient approach to investigate the boundary layer effect appearing in thin-body/coating structures.

1. Introduction

Isogeometric analysis (IGA), introduced by Hughes et al. [1] and further developed by Cottrell et al. [2,3], Bazilevs et al. [4,5], and Zhang et al. [6], has been an important numerical technique in the past decade. As far as we have known, Simpson et al. [7] first proposed the IGBEM and applied it to analyze elastostatic problem. After this, the IGBEM got more attention from many researchers who investigated various problems, e.g. 3D potential problems [8], fast multipole IGBEM [9], Helmholtz problems [10], ship wave-resistance problem [11,12], acoustic problems [13,14], shape optimization [15], nonsingular IGBEM analysis [16], weakly-singular integral equation [17], elasticity problems [18–20]. Recently, the isogeometric analysis is applied for the weakly singular symmetric Galerkin boundary element method (SGBEM) to analyze quasi-static elastic problems including crack problems in two-dimensional domains by B.H. Nguyen et al. in paper [21].

The main benefit of isogeometric method is that the geometry of the problem is preserved exactly. When building the models using CAD software, we can directly carry out numerical analysis based on the isogeometric method, i.e. there is no transformation from the CAD models to the computational meshes. In addition, the mesh refinement can be highly simplified using the standard knot-insertion and/or degree-elevation procedures [22] without communicating with the CAD system, once the initial mesh is completed.

In the computational models of thin-body/coating structures or the case when the calculation points are very close to the actual boundary, it is necessary to find one more accurate geometric approximation. As shown in Fig. 1, if the boundary of the thin-body/coating structures is discretized by using planar elements, e.g. *AB*, *CD* and *EF* or other approximate elements, the planar element *CD* (*EF*) will contact (pass through) the inner boundary. Furthermore, the inner boundary and some interior points very close to the real boundary may be located outside the boundary elements. Obviously, this calculation model is unreasonable. In contrast, the IGBEM in which exact boundary geometry remains can avoid the difficulties shown in Fig. 1. For thin-body/coating structures, the main difficulty is how to exactly calculate nearly singular integrals which has limited the application of the IGBEM in a lot of aspects, such as thin structures [23,24], contact problems [25], sensitivity problems [26] and crack problems [27].

In recent years, various methods have been proposed to deal with the nearly singular integrals appearing in conventional BEM. The proposed methods can be divided on the whole into two categories: ‘indirect algorithms’ and ‘direct algorithms’. The indirect algorithms [28–33], which benefit from the regularization ideas and techniques for the singular integrals, are mainly to calculate indirectly or avoid calculating the nearly singular integrals by establishing new regularized boundary integral equations (BIEs). The direct algorithms are to calculate the nearly singular integrals directly. They usually include interval subdivision method [34,35], special Gaussian quadrature method [36], and various coordinate transformations, which include polynomial transformation [37,38], degenerate mapping method [39],

* Corresponding author.
E-mail address: cydong@bit.edu.cn (C.Y. Dong).

http://dx.doi.org/10.1016/j.enganabound.2016.11.005
Received 12 September 2016; Received in revised form 13 November 2016; Accepted 21 November 2016
Available online 25 November 2016
0955-7997/

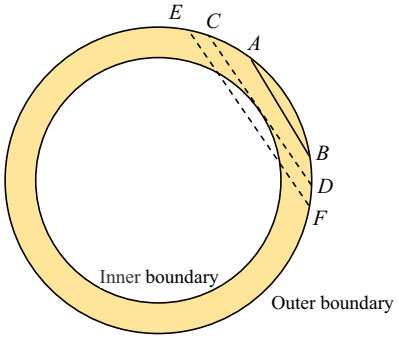

Fig. 1. Cutting plane of a thin-walled sphere.

coordinate optimal transformation [40], sigmoidal transformation [41,42], sinh transformation [42–44], rational transformation [45], distance transformation [46,47], exponential transformation [48–52], nonlinear coordinate transformation [53–55]. Among the mentioned techniques, the exponential transformation technique seems to be a more promising method for evaluating the nearly singular integrals. This method is based on the idea of diminishing the difference of the orders or the scale of change of addition factors in the denominator of the kernels. However, the technique how to exactly calculate near singular integrals appearing in the IGBEM is almost untouched.

In this paper, the exponential transformation method is used to remove or weaken the near singularities of nearly singular integrals appearing in the IGBEM. First, a formula of distance, based on the Taylor expansion, is expressed as $r^2 \approx d^2 + (\xi - \xi_p)^2 g_n(\xi)$ (2D problems) or $r^2 = d^2 + (\xi - \xi_p)^2 g_n^{11}(\xi) + (\eta - \eta_p)^2 g_n^{22}(\eta) + (\xi - \xi_p)(\eta - \eta_p) g_n^{12}(\xi, \eta)$ (3D problems), where ξ and η are the parametric coordinate, n is the order of Taylor's expansion, g_n and $g_n^{ij}(i, j = 1, 2)$ are well-behaved functions, ξ_p and η_p denote the position of the projection of the nearly singular point and d stands for the shortest distance from the calculation point to the element. Then the exponential transformation is combined with the distance formula to remove the near singularities of the considered integrals. Through the above transformation, nearly singular integrals over isogeometric elements can be evaluated with high accuracy, even when the nearly singular points lie at a position being very close to the boundary of computed model.

A brief outline of this paper is as follows. In Section 2 a short introduction into B-spline and NURBS are given, and the general form of nearly singular integrals for the IGBEM is described. The general form of 2D/3D nearly singular integrals represented by the distance function is given in Section 3. The next section presents the combination form of the exponential transformation and the distance function in detail. Numerical examples are given in Section 5 to verify the efficiency and accuracy of the present method.

2. Basic formulations

In this paper, we focus our attention on the computation of the boundary integrals with nearly singularity appearing in the IGBEM. Thus only some conclusions about the IGBEM are given, more details about the IGBEM can be found in [7,8]. First, a short introduction into B-spline and NURBS is given for completeness.

2.1. B-spline basis function

To define fully a B-spline the following three items are first required [1,7,8]:

- The curve degree p, e.g. linear ($p = 1$), quadratic ($p = 2$).
- A set of n control points P_i, here $P_i \in R^d$, $1 \le i \le n$, $d = 2$ or 3.
- A knot vector $U = \{\xi_1, \xi_2, \ldots, \xi_{n+p+1}\}$.

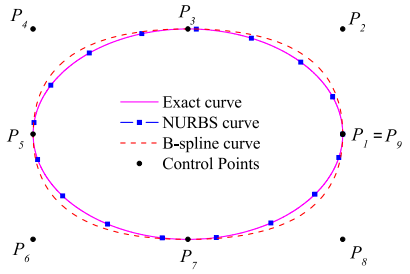

(a) The comparison of NURBS curve, B-spline and exact curve.

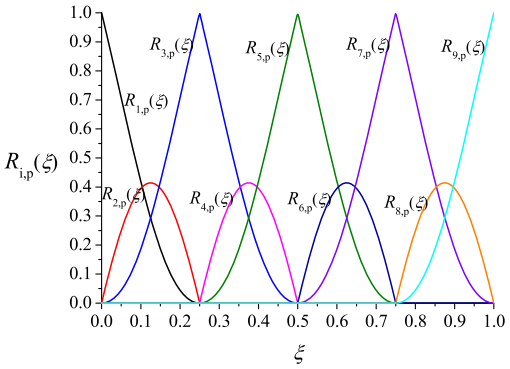

(b) The basis functions of the NURBS curve with $U = \{0,0,0,1\_4,1\_4,1\_2,1\_2,3\_4,3\_4,1,1,1\}$, $p = 2$ and $n = 9$.

Fig. 2. (a). The comparison of NURBS curve, B-spline and exact curve. (b) The basis functions of the NURBS curve with **U** = {0, 0, 0, 1/4, 1/4, 1/2, 1/2, 3/4, 3/4, 1, 1, 1}, $p = 2$ and $n = 9$.

Then the basis functions are denoted by $N_{i,p}$ with $1 \le i \le n$ and are defined as follows for $p = 0$

$$N_{i,0} = \begin{cases} 1 & \text{if } \xi_i \le \xi < \xi_{i+1}, \\ 0 & \text{otherwise,} \end{cases} \tag{1}$$

and for $p = 1, 2, 3, \cdots$:

$$N_{i,p} = \frac{\xi - \xi_i}{\xi_{i+p} - \xi_i} N_{i,p-1}(\xi) + \frac{\xi_{i+p+1} - \xi}{\xi_{i+p+1} - \xi_{i+1}} N_{i+1,p-1}(\xi) \tag{2}$$

Using these basis functions, it is easy to obtain the B-spline curve as follow

$$C(\xi) = \sum_{i=1}^{n} N_{i,p}(\xi) P_i \tag{3}$$

where ξ is the parametric coordinate that describes the Cartesian coordinates of vector $C(\xi)$ and $N_{i,p}(\xi)$ is the set of B-spline basis functions of degree p at ξ.

2.2. NURBS basis function

In CAD system, NURBS represents the dominant tool used to describe curves and surfaces. In fact, the B-spline can be considered as a sub-set of NURBS. The main difference between B-spline and NURBS is the counterparts by the use of an additional coordinate often referred to as a 'weighting', which makes the NURBS reproduce more complex curve and surface exactly. In NURBS each control point P_i is associated with a weighting ω_i leading to a set of NURBS basis functions denoted by $R_{i,p}(\xi)$.

The curve is then interpolated as

$$C(\xi) = \sum_{i=1}^{n} R_{i,p}(\xi) P_i \tag{4}$$

where the NURBS basis functions are given by

$$R_{i,p}(\xi) = \frac{N_{i,p}(\xi)\omega_i}{\sum_{j=1}^{n} N_{j,p}(\xi)\omega_j} \tag{5}$$

the $N_{i,p}(\xi)$ has been given in (2). Specially, when the weights are all set to unity (i.e.$\omega_i = 1, \ \forall\, i$), the basis functions given by (5) will reduce to the B-spline basis functions. In Fig. 2(a) we plot an ellipse to show the comparison of NURBS curve, B-spline and exact curve. The exact curve is obtained by the parameter equation $x = a\cos\theta, y = b\sin\theta$, where $a = 3, b = 1$ and $\theta \in [0,\ 2\pi]$. Both the B-spline and NURBS are created by the same knot vector $\mathbf{U} = \{0, 0, 0, 0.25, 0.25, 0.5, 0.5, 0.75, 0.75, 1, 1, 1\}$ and control points P_i $(i = 1,\ldots,9)$. Furthermore, the basis functions of NURBS curve in Fig. 2(a) are given in Fig. 2(b).

In our work, the isogeometric analysis relies on the use of the NURBS basis functions given above. We use the NURBS basis functions to describe the geometry of the problem to approximate the unknown fields in the governing PDEs. For potential problems, the potential u and normal derivative $\partial u/\partial n$ are approximated using NURBS basis functions.

2.3. The nearly integrals in the IGBEM

Considering the boundary integral equation of potential problems in the domain Ω enclosed by boundary Γ. The usual direct BEM formulation is presented as follow [52,56,57]:

$$c(\mathbf{y})u(\mathbf{y}) = \int_{\Gamma} q(\mathbf{x})u^*(\mathbf{x}, \mathbf{y})\, d\Gamma(\mathbf{x}) - \int_{\Gamma} u(\mathbf{x})q^*(\mathbf{x}, \mathbf{y})\, d\Gamma(\mathbf{x}) \tag{6}$$

where $\mathbf{y}$ and $\mathbf{x}$ are the source and the field points, respectively. c is a coefficient depending on the smoothness of the boundary at the source point $\mathbf{y}$. $u^*(\mathbf{x}, \mathbf{y})$ represents the fundamental solution for potential problems expressed as

$$\begin{aligned} u^*(\mathbf{x}, \mathbf{y}) &= -\tfrac{1}{2\pi}\ln r, \quad \text{for 2D problem} \\ u^*(\mathbf{x}, \mathbf{y}) &= \tfrac{1}{4\pi r}, \quad \text{for 3D problem} \end{aligned} \tag{7}$$

and $q^*(\mathbf{x}, \mathbf{y})$ is its normal derivative

$$q^*(\mathbf{x}, \mathbf{y}) = \frac{\partial u^*(\mathbf{x}, \mathbf{y})}{\partial r}\frac{\partial r}{\partial \mathbf{n}} \tag{8}$$

where r denotes the distance between the source and the field points and $\mathbf{n}$ is the unit outward normal direction to the boundary Γ, with components n_i, $i = 1, 2$ or. $i = 1, 2, 3$

In the implementation of 2D isogeometric BEM, we use the knot vector $\mathbf{U} = \{\xi_1, \xi_2, \ldots, \xi_{n+p+1}\}$, control points $\mathbf{P} = \{P_1, P_2, \ldots, P_n\}$ and curve order p to build the boundary shape and the basis functions. The unique elements of knot vector $\mathbf{U} = \{\xi_1, \xi_2, \ldots, \xi_{n+p+1}\}$ generate the discrete elements of the integral boundary. In order to carry out the numerical integration using Gauss-Lagendre quadrature, local coordinate $\hat{\xi}$ must be in the range $[-1, 1]$. Therefore, there should be a transformation from the parameter space $\xi \in [\xi_i,\ \xi_{i+1})$ (ξ_i is the i^{th} knot, i is the knot index) to the Gauss-Legendre range $[-1, 1]$, then the Jacobian value can be given as follow

$$J(\hat{\xi}) = \frac{d\Gamma}{d\hat{\xi}} = \frac{d\Gamma}{d\xi}\frac{d\xi}{d\hat{\xi}} \tag{9}$$

Thus, we can obtain the isogeometric boundary integral equation as follow

$$\begin{aligned} C(\mathbf{x}')\sum_{l=1}^{p+1} N_l^{\bar{e}}(\hat{\xi}')\, u^{le} + \sum_{e=1}^{N_e}\sum_{l=1}^{p+1}\left[\int_{-1}^{1} q^*(\mathbf{x}', \mathbf{x}(\hat{\xi}))N_l^e(\hat{\xi})J(\hat{\xi})d\hat{\xi}\right]u^{le} \\ = \sum_{e=1}^{N_e}\sum_{l=1}^{p+1}\left[\int_{-1}^{1} u^*(\mathbf{x}', \mathbf{x}(\hat{\xi}))N_l^e(\hat{\xi})J(\hat{\xi})d\hat{\xi}\right]q^{le} \end{aligned} \tag{10}$$

where $\mathbf{x}'$ represents the collocation points and $\hat{\xi}'$ represents the local coordinate of the collocation point in element $\bar{e}$. $N_b^e(\hat{\xi}) \equiv R_{i,p}(\xi(\hat{\xi}))$ is the local basis function that is related to the global basis functions. Since the NURBS basis functions do not necessarily obey the Kronecker-Delta property, therefore the u^{le} and q^{le} in Eq. (10) do not necessarily represent real potential and flux. The true potential and flux must be interpolated as follows

$$\begin{aligned} u(\mathbf{x}') &= \sum_{l=1}^{p+1} N_l^{\bar{e}}(\hat{\xi}')\, u^{l\bar{e}} \\ q(\mathbf{x}') &= \sum_{l=1}^{p+1} N_l^{\bar{e}}(\hat{\xi}')\, q^{l\bar{e}} \end{aligned} \tag{11}$$

In Eq. (10), when the evaluation point $\mathbf{y}$ is far from the integration elements, a straightforward application of Gaussian quadrature procedure suffices to evaluate such integrals accurately. However, when the evaluation point $\mathbf{y}$ is very close to the integration element Γ_e, the distance r between the evaluation point $\mathbf{y}$ and the integral element Γ_e is almost zero. Hence, nearly singular integrals appear in the discretized form of Eq. (10) and the numerical integrations by the standard Gaussian quadrature fail.

In this paper, we will use the exponential transformation method to deal with the boundary integrals with nearly singularity appearing in the IGBEM. The implementation is detailed in the following sections. For the sake of clarity and brevity for discussion, the following integrals in general form are used here.

$$I_1 = \int_{\Gamma_e} f(x, y)\ln r^2 d\Gamma, \quad I_2 = \int_{\Gamma_e} \frac{f(x, y)}{r^{2\alpha}}\, d\Gamma \tag{12}$$

where $r = \|x - y\|_2$, $\alpha > 0$ is a real constant and $f(x, y)$ denotes a well-behaved function.

3. Some issues on the distance function

In this section, we use the knot vector $\mathbf{U} = \{\xi_1, \xi_2, \ldots, \xi_{n+p+1}\}$. Both the geometry segment and boundary function are modeled by a continuous quadratic element ($p = 2$):

$$\begin{aligned} \mathbf{x}_e(\xi) &= \sum_{b=1}^{3} N_b^e(\xi)\mathbf{x}_b \\ u_e(\xi) &= \sum_{b=1}^{3} N_b^e(\xi)u_b \\ q_e(\xi) &= \sum_{b=1}^{3} N_b^e(\xi)q_b \end{aligned} \tag{13}$$

where $\xi \in U$, $\mathbf{x}_b$, u_b and q_b are vectors of the geometric coordinate, potential coefficient and flux coefficient, respectively, associated with the control point corresponding to the basis function b.

3.1. The distance function for 2D boundary elements

3.1.1. Determination of the projection point

The minimum distance d from the source point $\boldsymbol{y}$ to the integration element Γ_e is defined as the length $|\boldsymbol{y} - \boldsymbol{x}^p|$, where $\boldsymbol{x}^p$ is the projection point of $\boldsymbol{y}$ on integration element Γ_e. Letting ξ_p be the local coordinate of the projection point $\boldsymbol{x}^p$, i.e. $\boldsymbol{x}^p = (x_1(\xi_p), x_2(\xi_p))$.

Using the relation $r_i = x_i(\xi) - y_i$, one has $r^2 = \|\boldsymbol{x} - \boldsymbol{y}\|_2^2 = r_i r_i$. When $\xi = \xi_p$, r^2 reaches the minimum value, thus we have

$$[x_i(\xi_p) - y_i]\frac{\partial x_i}{\partial \xi} = 0, \quad i = 1, 2 \tag{14}$$

Here, the summation convention is used, and $\frac{\partial x_i}{\partial \xi} = \frac{\partial x_i}{\partial \xi}\Big|_{\xi=\xi_p}$, $i = 1, 2$.

If the source point $\boldsymbol{y}$ is sufficiently close to the boundary element Γ_e, then $\boldsymbol{x}^p$ is inside the integration element, and Eq. (14) has a unique real root $\xi_p \in [\xi_i,\ \xi_{i+1})$. The real root ξ_p can be evaluated by using the Newton iteration method. Setting

$$f(\xi_p) = [x_i(\xi_p) - y_i]\frac{\partial x_i}{\partial \xi}. \tag{15}$$

The formula of Newton iteration method can be expressed as

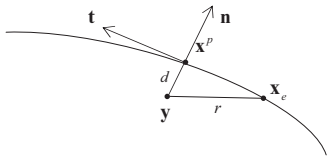

Fig. 3. The minimum distance d from the source point $\boldsymbol{y}$ to the element.

follow:

$$\xi_p^{(k+1)} = \xi_p^{(k)} - \frac{f(\xi_p^{(k)})}{f'(\xi_p^{(k)})} \tag{16}$$

where $k \geq 0$ and $\xi_p^{(0)}$ is a given value.

3.1.2. Distance function r^2 for 2D boundary elements

As shown in Fig. 3, the minimum distance d from the source point to the element is defined as perpendicular to the tangential surface, through the nearly singular point $\boldsymbol{x}^p$ and the source point $\boldsymbol{y}$. $\mathbf{x}_e(\xi)$ is polynomial with respect to ξ. Applying the Taylor's expansion of $\mathbf{x}_e(\xi)$ in the neighborhood of projection point $\boldsymbol{x}^p$ in the parameter plane, we have

$$\mathbf{x}_e(\xi) = \mathbf{x}_e(\xi_p) + (\xi - \xi_p)\frac{d}{d\xi}\mathbf{x}_e + \frac{1}{2}(\xi - \xi_p)^2\frac{d^2}{d\xi^2}\mathbf{x}_e + \ \ldots + \frac{1}{n!}(\xi - \xi_p)^n\frac{d^n}{d\xi^n}\mathbf{x}_e + \cdots \tag{17}$$

where

$$\frac{d^n}{d\xi^n}\mathbf{x}_e(\xi) = \sum_{b=1}^{p+1}\frac{d^n}{d\xi^n}N_b^e(\xi)\mathbf{x}_b, \ \ N_b^e(\hat{\xi}) \equiv R_{i,p}(\xi(\hat{\xi})).$$

The first order derivative of NURBS basis function is expressed as [18]

$$\frac{d}{d\xi}R_{i,p}(\xi) = \omega_i\frac{W(\xi)N'_{i,p}(\xi) - W'(\xi)N_{i,p}(\xi)}{(W(\xi))^2} \tag{18}$$

where $N_{i,p}(\xi)$ is the B-spline basis function, $N'_{i,p}(\xi) = \frac{d}{d\xi}N_{i,p}(\xi)$ and $W'(\xi) = \sum_{j=1}^{n}N'_{j,p}(\xi)\omega_j$.

The higher-order derivatives of the rational function can be expressed in terms of lower-order derivatives as [18]

$$\frac{d^k}{d\xi^k}R_{i,p}(\xi) = \frac{A_i^{(k)}(\xi) - \sum_{b=1}^{k}\binom{k}{b}W^{(b)}(\xi)\frac{d^{(k-b)}}{d\xi^{(k-b)}}R_{i,p}(\xi)}{W(\xi)} \tag{19}$$

where $\binom{k}{b} = \frac{k!}{b!\,(k-b)!}$, $A_i^{(k)}(\xi) = \omega_i\frac{d^k}{d\xi^k}N_{i,p}(\xi)$.

Because the NURBS basis is rational polynomial, there will be an $O(\xi - \xi_p)^n$ in Eq. (17). Particularly, when the weights are all set to unity (i.e. $\omega_i = 1, \quad \forall\, i$), the $O(\xi - \xi_p)^n$ will vanish.

Using Eq. (17), the distance square r^2 between the source point $\boldsymbol{y}$ and the field point $\mathbf{x}_e$ (ξ) can be written as

$$r^2(\xi) = [\mathbf{x}_e(\xi) - \mathbf{y}][\mathbf{x}_e(\xi) - \mathbf{y}] = d^2 + (\xi - \xi_p)^2 g_n(\xi) \tag{20}$$

where $d^2 = (\mathbf{y} - \mathbf{x}^p)(\mathbf{y} - \mathbf{x}^p)$, and $g_n(\xi)$ is a function associated with the Taylor's expansion in Eq. (17).

For $n = 3$

$$g_3(\xi) = (\mathbf{x}'_e)^2 + (\xi - \xi_p)\mathbf{x}'_e\mathbf{x}_e^{(2)} + \frac{1}{4}(\xi - \xi_p)^2(\mathbf{x}_e^{(2)})^2 + \frac{1}{3}(\xi - \xi_p)^2\frac{dx_e}{d\xi}\mathbf{x}'_e\mathbf{x}_e^{(3)} + \frac{1}{6}(\xi - \xi_p)^3\mathbf{x}_e^{(2)}\mathbf{x}_e^{(3)} + \frac{1}{36}(\xi - \xi_p)^4(\mathbf{x}_e^{(3)})^2 \tag{21}$$

where $\mathbf{x}_e^{(n)} = \frac{d^n\mathbf{x}_e}{d\xi^n}$.

For higher order Taylor's expansion, more coefficients need to be derived following the above procedure. The detailed forms of $g_4(\xi), \ldots, g_8(\xi)$ are given in Appendix A. In fact, sufficiently high precision can be gained by $g_8(\xi)$ for general physics problems.

3.1.3. Nearly singular integrals on the elements

Considering the nearly singular integrals I_1 over element Γ_e $([\xi_i, \ \xi_{i+1}])$, we have

$$I_1 = \int_{\xi_i}^{\xi_{i+1}} f(\xi)\ln r^2 d\xi = \int_{\xi_i}^{\xi_p} f(\xi)\ln r^2 d\xi + \int_{\xi_p}^{\xi_{i+1}} f(\xi)\ln r^2 d\xi \tag{22}$$

where ξ_p is the projection point and the Jacobian of transformation is included in $f(\xi)$. Then, using $\mu = \xi_p - \xi$ for the first integral and $\mu = \xi - \xi_p$ for the second integral on the right-hand of Eq. (22) gives

$$I_1 = \int_0^{\xi_p - \xi_i} f(\mu)\ln r^2 d\mu + \int_0^{\xi_{i+1} - \xi_p} f(\mu)\ln r^2 d\mu \tag{23}$$

Similarly

$$I_2 = \int_0^{\xi_p - \xi_i}\frac{f(\mu)}{r^\alpha}d\mu + \int_0^{\xi_{i+1} - \xi_p}\frac{f(\mu)}{r^\alpha}d\mu \tag{24}$$

Thus, the nearly singular integrals in Eq. (12) can be reduced to the following forms:

$$I_1 = \int_0^A f(\mu)ln(d^2 + \mu^2 g(\mu))d\mu \tag{25}$$

$$I_2 = \int_0^A \frac{f(\mu)}{[d^2 + \mu^2 g(\mu)]^\alpha}d\mu \tag{26}$$

where $A = \xi_p - \xi_i$ or $\xi_{i+1} - \xi_p$, which changes with the integral elements; $f(\cdot)$ is a smooth function that consists of shape function, Jacobian and coefficients from the derivative of the integral kernels.

3.2. The distance function for 3D boundary elements

3.2.1. Determination of the projection point

For 3D problems, the minimum distance d from the source point $\boldsymbol{y}$ to the integration element $\Gamma_e([\xi_i, \xi_{i+1}) \times [\eta_j, \eta_{j+1}))$ is defined as the length $|\boldsymbol{y} - \boldsymbol{x}^p|$, where $\boldsymbol{x}^p$ is the projection point of $\boldsymbol{y}$ on integration element Γ_e. Letting $(\xi_p, \ \eta_p)$ be the local coordinates of the projection point $\boldsymbol{x}^p$, i.e. $\boldsymbol{x}^p = (x_1(\xi_p, \eta_p), x_2(\xi_p, \eta_p), x_3(\xi_p, \eta_p))$, then ξ_p and η_p are the real roots of the following equations

$$\begin{cases}[x_i(\xi_p, \eta_p) - y_i]\frac{\partial x_i}{\partial \xi} = 0 \\ [x_i(\xi_p, \eta_p) - y_i]\frac{\partial x_i}{\partial \eta} = 0\end{cases}, \quad i = 1, 2, 3 \tag{27}$$

If the source point $\boldsymbol{y}$ is sufficiently close to the boundary Γ_e, then $\boldsymbol{x}^p$ is inside the integration element, and Eq. (27) has a pair of the unique real roots $(\xi_p, \ \eta_p) \in [\xi_i, \xi_{i+1}) \times [\eta_j, \eta_{j+1})$. The real roots $\xi_p, \ \eta_p$ can be evaluated numerically by using the Newton's method. Setting

$$f_1(\xi_p, \eta_p) = [x_i(\xi_p, \eta_p) - y_i]\frac{\partial x_i}{\partial \xi}, \ \ f_2(\xi_p, \eta_p) = [x_i(\xi_p, \eta_p) - y_i]\frac{\partial x_i}{\partial \eta} \tag{28}$$

The formula of the Newton's method can be expressed as

$$F'(\boldsymbol{\eta}^{(k)})\Delta\boldsymbol{\eta}^{(k)} = -F(\boldsymbol{\eta}^{(k)}) \tag{29}$$

where

$$\Delta\boldsymbol{\eta}^{(k)} = \boldsymbol{\eta}^{(k+1)} - \boldsymbol{\eta}^{(k)}, \ \boldsymbol{\eta}^{(k)} = (\xi_p^{(k)}, \eta_p{}^{(k)})^{\mathrm{T}}, \quad \boldsymbol{\eta}^{(k+1)} = (\xi_p^{(k+1)}, \eta_p{}^{(k+1)})^{\mathrm{T}},$$

$$F(\boldsymbol{\eta}^{(k)}) = \begin{bmatrix} f_1(\xi_p^{(k)}, \eta_p{}^{(k)}) \\ f_2(\xi_p^{(k)}, \eta_p{}^{(k)}) \end{bmatrix}, \ F'(\boldsymbol{\eta}^{(k)}) = \begin{bmatrix} \frac{\partial f_1}{\partial \xi_p} & \frac{\partial f_1}{\partial \eta_p} \\ \frac{\partial f_2}{\partial \xi_p} & \frac{\partial f_2}{\partial \eta_p} \end{bmatrix}_{\boldsymbol{\eta} = \boldsymbol{\eta}^{(k)}}$$

3.2.2. Distance function r^2 for 3D boundary elements

As shown in Fig. 4, the minimum distance d from the source point

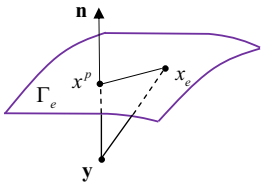

Fig. 4. The minimum distance d from the source point $\boldsymbol{y}$ to the 3D element.

to the element is defined as being perpendicular to the tangential surface, through the nearly singular point $\boldsymbol{x}^p$ and the source point $\boldsymbol{y}$. $\mathbf{x}_e(\xi, \eta)$ is polynomial with respect to ξ and η. Applying the Taylor's expansion of $\mathbf{x}_e(\xi, \eta)$ in the neighborhood of projection point $\boldsymbol{x}^p$ in the parameter plane, we have

$$\mathbf{x_e}(\xi, \eta) = \mathbf{x_k}(\xi_p, \eta_p) + (\xi - \xi_p)\frac{\partial \mathbf{x_e}}{\partial \xi} + (\eta - \eta_p)\frac{\partial \mathbf{x_e}}{\partial \eta} + \frac{1}{2}\left((\xi - \xi_p)\frac{\partial}{\partial \xi} + (\eta - \eta_p)\frac{\partial}{\partial \eta}\right)^2 \mathbf{x_e} + \frac{1}{6}\left((\xi - \xi_p)\frac{\partial}{\partial \xi} + (\eta - \eta_p)\frac{\partial}{\partial \eta}\right)^3 \mathbf{x_e} + \ldots \tag{30}$$

where

$$\frac{\partial^{k+l}}{\partial \xi^k \partial \eta^l}\mathbf{x}_e(\xi, \eta) = \sum_{b=1}^{(p+1)\times(q+1)} \frac{\partial^{k+l}}{\partial \xi^k \partial \eta^l} N_b^e(\xi, \eta)\mathbf{x}_b, \quad N_b^e(\hat{\xi}, \hat{\eta}) \equiv R_{i,p}(\xi(\hat{\xi}), \eta(\hat{\eta})) \tag{31}$$

Using Eq. (30), the distance square r^2 between the source point $\boldsymbol{y}$ and the field point $\mathbf{x}_e$ (ξ, η) can be written as

$$r^2(\xi, \eta) = [\mathbf{x}_e(\xi, \eta) - \mathbf{y}][\mathbf{x}_e(\xi, \eta) - \mathbf{y}] = d^2 + (\xi - \xi_p)^2 g_{11}(\xi) + (\eta - \eta_p)^2 g_{22}(\eta) + (\xi - \xi_p)(\eta - \eta_p) g_{12}(\xi, \eta) \tag{32}$$

where $d^2 = (\mathbf{y} - \mathbf{x}^p)(\mathbf{y} - \mathbf{x}^p)$, and $g_{11}(\xi)$, $g_{22}(\eta)$, $g_{12}(\xi, \eta)$ are functions associated with the Taylor's expansion in Eq. (30).

3.2.3. Nearly singular integrals on the elements

Considering the nearly singular integrals I_3 over element Γ_e $([\xi_i, \xi_{i+1}) \times [\eta_j, \eta_{j+1}))$, we have

$$\begin{aligned} I_3 &= \int_{\eta_j}^{\eta_{j+1}} \int_{\xi_i}^{\xi_{i+1}} \frac{f(\xi, \eta)}{r^{2\alpha}} d\xi d\eta \\ &= \int_{\eta_j}^{\eta_p} \int_{\xi_i}^{\xi_p} \frac{f(\xi, \eta)}{r^{2\alpha}} d\xi d\eta + \int_{\eta_j}^{\eta_p} \int_{\xi_p}^{\xi_{i+1}} \frac{f(\xi, \eta)}{r^{2\alpha}} d\xi d\eta + \int_{\eta_p}^{\eta_{j+1}} \int_{\xi_i}^{\xi_p} \frac{f(\xi, \eta)}{r^{2\alpha}} d\xi d\eta \\ &\quad + \int_{\eta_p}^{\eta_{j+1}} \int_{\xi_p}^{\xi_{i+1}} \frac{f(\xi, \eta)}{r^{2\alpha}} d\xi d\eta \end{aligned} \tag{33}$$

where ξ_p, η_p are the projection point and the Jacobian of transformation is included in $f(\xi, \eta)$. Then, using $\mu = \xi_p - \xi$, $v = \eta_p - \eta$ for the first integral, $\mu = \xi - \xi_p$, $v = \eta_p - \eta$ for the second integral, $\mu = \xi_p - \xi$, $v = \eta - \eta_p$ for the third integral and $\mu = \xi - \xi_p$, $v = \eta - \eta_p$ for the forth integral on the right-hand of Eq. (33) gives

$$\begin{aligned} I_3 &= \int_0^{\eta_p - \eta_j} \int_0^{\xi_p - \xi_i} \frac{f(\mu, v)}{r^{2\alpha}} d\mu dv + \int_0^{\eta_p - \eta_j} \int_0^{\xi_{i+1} - \xi_p} \frac{f(\mu, v)}{r^{2\alpha}} d\mu dv \\ &\quad + \int_0^{\eta_{j+1} - \eta_p} \int_0^{\xi_p - \xi_i} \frac{f(\mu, v)}{r^{2\alpha}} d\mu dv + \int_0^{\eta_{j+1} - \eta_p} \int_0^{\xi_{i+1} - \xi_p} \frac{f(\mu, v)}{r^{2\alpha}} d\mu dv \end{aligned} \tag{34}$$

Thus, the nearly singular integrals in Eq. (12) can be reduced to the following form:

$$I = \int_0^B \int_0^A \frac{f(\mu, v)}{[d^2 + \mu^2 g_{11}(\mu) + v^2 g_{22}(v) + \mu v g_{12}(\mu, v)]^\alpha} d\mu dv \tag{35}$$

where $A = \xi_p - \xi_i$ or $\xi_{i+1} - \xi_p$ and $B = \eta_p - \eta_j$ or $\eta_{j+1} - \eta_p$ which changes with the integral elements; $f(\cdot)$ is a smooth function that consists of shape function, Jacobian and coefficients from the derivative of the integral kernels.

4. Combination of the distance function and exponential transformation

The exponential transformation has been proved to be feasible in dealing with the nearly singular integrals in conventional BEM [48–52]. In this paper, the exponential transformation will be used to treat the nearly singular integrals in the IGBEM. Different from the conventional BEM, parametric elements in IGBEM are defined by the knot vectors U and **V**. Therefore, the constants A $(=\xi_{i+1} - \xi_p$ or $\xi_p - \xi_i)$ and B $(=\eta_{j+1} - \eta_p$ or $\eta_p - \eta_j)$ in the following exponential transformations will contain the values (ξ_i or η_j, $i = 1, 2, \ldots, n + p + 1$ and $j = 1, 2, \ldots, m + q + 1$) of knot vector which will be a difference with the conventional BEM.

4.1. Combination of the distance function and exponential transformation for 2D problem

The integrals in Eqs. (25) and (26) can be accurately evaluated using the exponential transformation technique. Since Gaussian quadrature is often used in evaluating boundary element integrals, this study generalizes the exponential transformation by

$$\mu = d(e^{k(1+t)} - 1), \quad -1 \le t \le 1 \tag{36}$$

where $k = \frac{1}{2}\ln(1 + \frac{A}{d})$.

The Jacobian of the transformation (36) is then given by $|J| = kde^{k(1+t)}$.

Substituting (36) into Eqs. (25) and (26), we obtain the following equations

$$I_1 = dk \ln d^2 \int_{-1}^{1} f(t) e^{k(1+t)} dt + dk \int_{-1}^{1} f(t) e^{k(1+t)} \ln(1 + (e^{k(1+t)} - 1)^2 g(t)) dt \tag{37}$$

$$I_2 = \frac{k}{d^{2\alpha - 1}} \int_{-1}^{1} \frac{f(t) e^{k(1+t)}}{[1 + (e^{k(1+t)} - 1)^2 g(t)]^\alpha} dt \tag{38}$$

By following the procedure described above, the near singularity of the boundary integrals has been fully regularized. The final integral formulations over curved boundary elements are obtained as shown in Eqs. (37) and (38), which can be computed straightforwardly by using standard Gaussian quadrature.

4.2. Combination of the distance function and exponential transformation for 3D problem

The surface nearly singular integrals can be accurately evaluated using the presented technique. Since Gaussian quadrature is often used in evaluating boundary element integrals, this study generalizes the exponential transformation by

$$\begin{aligned} \mu &= d(e^{m_1 + m_2 s} - 1), \\ v &= d(e^{n_1 + n_2 t} - 1), \end{aligned} \tag{39}$$

where $-1 \le s \le 1$, $-1 \le t \le 1$ and $m_1 = m_2 = \frac{1}{2}\ln(1 + \frac{A}{d})$, $n_1 = n_2 = \frac{1}{2}\ln(1 + \frac{B}{d})$.

The Jacobian of the transformation (39) is then given by $|J| = d^2 m_2 n_2 e^{m_1 + n_1 + m_2 s + n_2 t}$.

Substituting (39) into Eq. (35), we obtain the following equation

$$I = \frac{1}{4\pi} \frac{1}{d^{2\alpha - 2}} \int_{-1}^{1} \int_{-1}^{1} \frac{f(s, t) m_2 n_2 e^{m_1 + n_1 + m_2 s + n_2 t}}{F(s, t)} |J| ds dt \tag{40}$$

where $F(s, t) = [1 + (e^{m_1 + m_2 s} - 1)^2 g_n^{11}(s, t) + (e^{n_1 + n_2 t} - 1)^2 g_n^{22}(s, t) + (e^{m_1 + m_2 s} - 1)(e^{n_1 + n_2 t} - 1) g_n^{12}(s, t)]^\alpha$

By following the procedure described above, the near singularity of the 3D boundary integrals can be fully regularized. The final integral formulations over the surface boundary elements are obtained as shown in Eq. (40), which can be computed straightforwardly by using standard Gaussian quadrature.

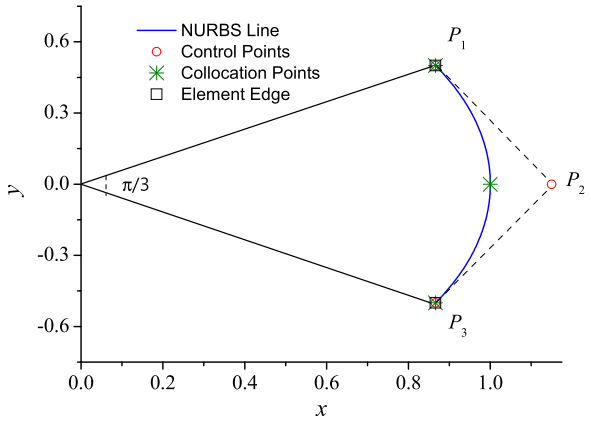

Fig. 5. The isogeometric model of the integral segment.

5. Numerical examples

In this section, several numerical examples involving boundary layer effect are investigated using the IGBEM. Numerical results are correctly obtained even when the distance between the evaluation point and the real boundary of the model is very small. The present results and those from the conventional algorithm (without any transformation) and the exact solutions are all presented for comparison. In order to carry out accuracy and convergence analysis, an average relative error is given as

$$\text{Relative Error (RE)} = \frac{|I^k_{num} - I^k_{exact}|}{|I^k_{exact}|} \tag{41}$$

where I^k_{num} and I^k_{exact} denote the numerical and exact values at the k th point, respectively. Since some of the integrals described above are not amenable to analytic integration, the exact values for these integrals are replaced by the values using the subdivision method.

Table 1
Results of I_1 when the computed points are gradually close to the real boundary.

(x, y)	d/L	Reference	No Transformation	Present solution	Error
(0.9, 0)	0.095493	0.23451461E+00	0.23451013E+00	0.23451509E+00	2.0467808E−06
(0.99, 0)	0.0095493	0.27098278E+00	0.26599937E+00	0.27098326E+00	1.7713303E−06
(0.999, 0)	0.00095493	0.27472384E+00	0.26614927E+00	0.27472432E+00	1.7472091E−06
(0.9999, 0)	0.000095493	0.27509876E+00	0.26608342E+00	0.27509923E+00	1.7084773E−06
(0.99999, 0)	0.0000095493	0.27513626E+00	0.26607601E+00	0.27513673E+00	1.7082445E−06
(0.999999, 0)	0.00000095493	0.27514001E+00	0.26607526E+00	0.27514048E+00	1.7082212E−06

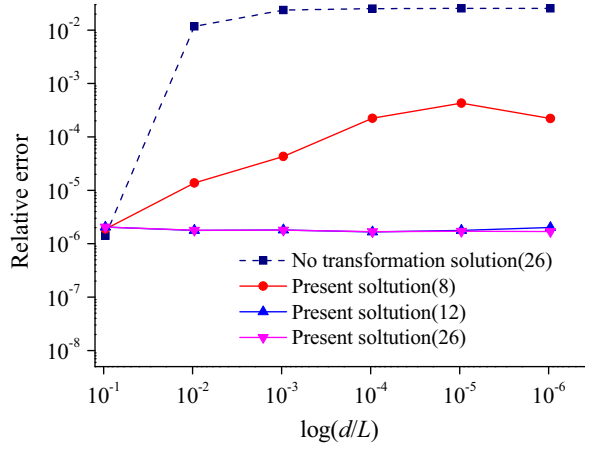

Fig. 6. Numerical results of I_1 from the present method with 8, 12 and 26 Gaussian points.

5.1. Nearly weakly singular integrals

We consider following integral

$$I_1 = \int_{\Gamma_e} u^* d\Gamma \tag{42}$$

which is representative of the nearly singulars in the IGBEM of 2D Laplacian problems. As shown in Fig. 5, the integral segment Γ_e is the arc of the unit circle with an angle of $\frac{\pi}{3}$ and $r = \sqrt{(x - x_0)^2 + (y - y_0)^2}$ with (x_0, y_0) being the coordinate at the calculated point $\boldsymbol{x}_0$ and (x, y) the coordinate of general points $\boldsymbol{x}$ along the boundary element. The element is represented as a quadratic NURBS curve with knot sequence $\mathbf{U} = \{0, 0, 0, 1, 1, 1\}$, control points $P_1(\sqrt{3}/2, 1/2)$, $P_2(2/\sqrt{3}, 0)$ and $P_3(\sqrt{3}/2, -1/2)$ as well as weights $[1, \sqrt{3}/2, 1]$. The coordinate at the calculation point is chosen as $(x_0, y_0) = (r_0, \theta_0)$, in which r_0 varies from 0.9 to 0.999999 and $\theta_0 = 0$. In this paper, the dimensionless distance, d/L, is used in most of the computed results, where L stands for the

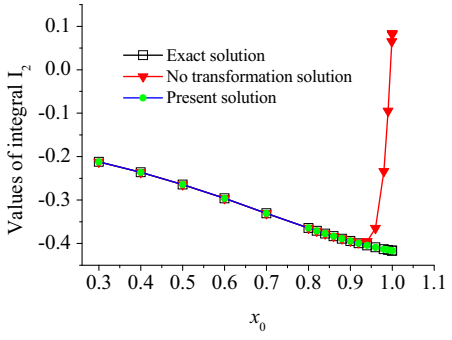

(a) The results of I_2 when x_0 is gradually close to the boundary

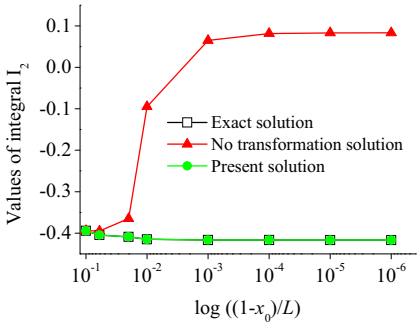

(b) The results of I_2 when x_0 is very close to the real boundary

Fig. 7. Results of I_2 for various distances to the real boundary. (a) The results of I_2 when x_0 is gradually close to the boundary. (b) The results of I_2 when x_0 is very close to the real boundary.

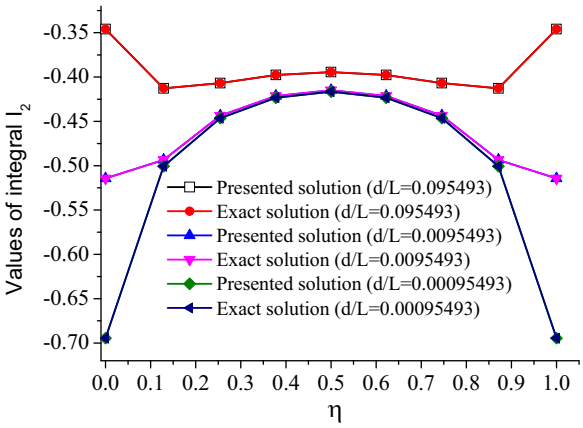

Fig. 8. The results of integral I_2 when the nearly singular points for fixed d/L are moving along the boundary.

integration span since the dimensionless distance reflects the closeness of the source point to the integration more essentially. For this example, L is $\frac{\pi}{3}$. Thus, the value of dimensionless distance d/L is in the orders of 9.5493×10^{-2} to 9.5493×10^{-8}, which is thought to be enough for general computational applications.

The numerical results of integral I_1 are listed in Table 1 from which it can be seen that the conventional IGBEM (no transformation) and the present method are both efficient when the dimensionless distance $d/L \geq 0.095493$, but the conventional IGBEM fails when the internal points are much closer to the boundary. In contrast, the results from the present method are excellently consistent with the exact solutions even in the very unfavorable computational condition $d/L = 0.00000095493$.

Fig. 6 shows the relative errors for the integral I_1 as the computed points are gradually close to the element. When the computed points are not very close to the boundary (e.g.$d/L \geq 0.095493$), both the conventional Gaussian quadrature and the present method are efficient and can yield accurate results. However, with the decrease of the dimensionless distance d/L, the conventional Gaussian quadrature performs less satisfactory. In contrast, the present method improves the accuracy of the numerical evaluation of the nearly singular integral even when the dimensionless distance d/L is very small.

5.2. Nearly strongly singular integrals

Next, consider the following integral

$$I_2 = \int_{\Gamma_e} \frac{\partial u^*}{\partial x} d\Gamma \tag{43}$$

where the integral segment Γ_e and r remain the same as the above example. The coordinate at the calculation point is chosen as $(x_0, y_0) = (r_0, 0)$ where r_0 varies from 0.9 to 0.999999. The results of the integral I_2 are shown in Fig. 7(a) for various distances to the boundary, and the results at the points very close to the real boundary are displayed in more detail in Fig. 7(b).

It can be clearly seen from Fig. 7(a) and (b) that both conventional method and present method can produce accurate results when $x_0 \leq 0.9$. However, when $x_0 > 0.9$, the results obtained by the conventional IGBEM become less satisfactory or even invalid. In contrast, the results from the present method are well consistent with the exact solutions as x_0 varies from 0.9 to 0.999999.

Fig. 8 shows the results of integral I_2 when the nearly singular points for fixed dimensionless distance d/L are moving along the boundary. One can see that the present method is insensitive to the position of the nearly singular point, even near the end points of the calculation interval.

To investigate the results influenced by the order of the Taylor expansion, Table 2 lists the relative errors of the results computed by different orders of Taylor expansion. In general, the higher order of Taylor expansion can improve the accuracy of the numerical evaluation of the nearly singular integrals. With the computed points being much closer to the real boundary, the higher order of Taylor expansion will be needed.

5.3. Highly nearly singular boundary integrals over a rectangular region

To test our method and program, the following surface integral over a 3D rectangular element with $x \in [0, 2]$, $y \in [0, 4]$ (Fig. 9) is considered. The corresponding polynomial orders and knot vectors are given in Table 3 and control points are given in Table 4.

$$I_3(\mathbf{x}^p) = \frac{1}{4\pi} \int_0^4 \int_0^2 \frac{1}{r^\beta} dxdy \tag{44}$$

The source points with coordinates $(1, 1, z)$ are computed, and the projection point of the source points is x^p with intrinsic coordinates $\xi_p = 0.5$, $\eta_p = 0.25$. Table 5 lists the computed results for nearly singularity orders of β from 1 to 3. Analytical results are easy to obtain for this example and are also listed in Table 5, which shows that the computed values are in excellent agreement with the analytical results. In this example, the weights of the control points are 1.0, so the Taylor expansion are exact.

5.4. Nearly singular boundary integrals over a curved boundary element

The fourth example is concerned with the following nearly singular over a 3D curved boundary element. The element is a 90° cylindrical panel with $r = 1$, $l = 2$ as shown in Fig. 10. The corresponding polynomial orders and knot vectors are given in Table 6 and control points are given in Table 7. Here, the dimensionless distance is also defined as d/L, while L stands for the biggest integration span. Therefore, L equals 2 for this example.

$$I_4 = \int_{\Gamma_e} \frac{1}{4\pi r} d\Gamma \tag{45}$$

The point $\boldsymbol{x}$ being close to the element with coordinates $(r_0 \cos\frac{\pi}{4}, 1, r_0 \sin\frac{\pi}{4})$, where r_0 varies from 0.9 to 0.999999, is computed in this example. Obviously, the projection point of $\boldsymbol{x}$ is $x^p(\cos\frac{\pi}{4}, 1, \sin\frac{\pi}{4})$ with intrinsic coordinates $\xi_p = 0.5$, $\eta_p = 0.5$. Fig. 11 shows the results of integral I_4 when computed points are

Table 2
The results from different orders of Taylor expansion.

(x_1, x_2)	d/L	Reference	2 tems	4 tems	6 tems	8 tems
(0.9, 0)	0.095493	0.39436560E+00	5.6144603E−03	7.1279037E−05	3.0428618E−07	7.6071544E−08
(0.99, 0)	0.0095493	0.41484624E+00	7.0585670E−03	3.6071196E−04	1.8729831E−05	1.0606339E−06
(0.999, 0)	0.00095493	0.41648888E+00	8.6516836E−03	3.9902626E−04	2.0432718E−05	1.0084303E−06
(0.9999, 0)	0.000095493	0.41664893E+00	8.8119751E−03	4.0499324E−04	1.8360782E−05	3.2641389E−06
(0.99999, 0)	0.0000095493	0.41666489E+00	8.8334057E−03	4.0022571E−04	2.3520100E−05	1.8720080E−06
(0.999999, 0)	0.00000095493	0.41666652E+00	8.8755391E−03	3.5976013E−04	6.4032023E−05	4.2384015E−05

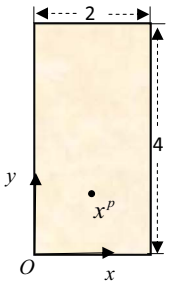

Fig. 9. The isogeometric rectangular surface element.

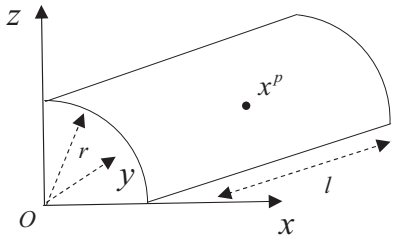

Fig. 10. 3D isogeometric cylindrical surface element.

Table 3
Polynomial orders and knot vectors for the isogeometric boundary element.

Direction	Order	Knot vector
ξ	$p = 2$	$\mathbf{U} = \{0, 0, 0, 1, 1, 1\}$
η	$q = 2$	$\mathbf{V} = \{0, 0, 0, 1, 1, 1\}$

Table 4
Control points for the element.

Control points	Coordinates	Weights
P_1	(0,0,0)	1
P_2	(1,0,0)	1
P_3	(2,0,0)	1
P_4	(0,2,0)	1
P_5	(1,2,0)	1
P_6	(2,2,0)	1
P_7	(0,4,0)	1
P_8	(1,4,0)	1
P_9	(2,4,0)	1

Table 6
Polynomial orders and knot vectors for the isogeometric boundary element.

Direction	Order	Knot vector
ξ	$p = 2$	$\mathbf{U} = \{0, 0, 0, 1, 1, 1\}$
η	$q = 2$	$\mathbf{V} = \{0, 0, 0, 1, 1, 1\}$

Table 7
Control points for the element.

Control points	Coordinates	Weights
P_1	(1,0,0)	1
P_2	(1,1,0)	1
P_3	(1,2,0)	1
P_4	(1,0,1)	$\sqrt{2}/2$
P_5	(1,1,1)	$\sqrt{2}/2$
P_6	(1,2,1)	$\sqrt{2}/2$
P_7	(0,0,1)	1
P_8	(0,1,1)	1
P_9	(0,2,1)	1

moving closer to the boundary element. One can see that the present method is effective to the 3D curved element. Here, although the results are obtained by 6 order Taylor expansion (Eq. (30)), the results are consistent with the exact solutions very well.

5.5. Boundary layer effect in a plate

A 2D circular plate with radius 1.0 is considered as shown in Fig. 12. The prescribed boundary condition is $u = 2x + y$. In this case, the circular plate boundary is represented as a quadratic NURBS curve with knot sequence $\mathbf{U} = \{0, 0, 0, 1, 1, 2, 2, 3, 3, 4, 4, 4\}$ and control points $P_1(1, 0)$, $P_2(\sqrt{2}/2, \sqrt{2}/2)$, $P_3(0, 1)$, $P_4(-\sqrt{2}/2, \sqrt{2}/2)$, $P_5(-1, 0)$, $P_6(-\sqrt{2}/2, -\sqrt{2}/2)$, $P_7(0, -1)$, $P_8(\sqrt{2}/2, -\sqrt{2}/2)$ and $P_9 = P_1$. Here, the boundary functions are also approximated by using quadratic NURBS interpolation.

The numerical results of potential are shown in Table 8, from which it can be seen that when the calculated point is not very close to the boundary, all the schemes are efficient and can yield accurate results. However, the conventional IGBEM fails when the internal point becomes much closer to the boundary. In contrast, the results from the present method are excellently consistent with the analytical solutions even when the distance d/L is as small as 6.3661977×10^{-9}, which will meet engineering requirements. Fig. 13 plots the convergence curve of the potential at the point $(d \cos\theta, d \sin\theta)$, where $\theta = \pi/4$ and $d = r - r_0$, which shows that the convergence rate of the present method is fast even when the dimensionless distance d/L between the computed point and the boundary approaches 6.3661977×10^{-9}.

Furthermore, as shown in Fig. 14, 60 interior points along the circumferential uniform distribution are taken into account. The parametric equation of the points is $x = r_0 \cos\theta$, $y = r_0 \sin\theta$. Thus the distance d to the real boundary can be expressed as $d = r - r_0$. In Fig. 15, the results obtained by the present method and the conventional algorithm (without transformation) as well as the exact solutions are all given for comparison. It can be clearly seen from Fig. 15(a) that all the methods can lead to accurate results when the dimensionless distance is $d/L = 6.3661977 \times 10^{-2}$. However, when the distance is

Table 5
Computed results for various values of β at source points.

	β=1			β=2			β=3		
z	Analytical	Current	No transform	Analytical	Current	No transform	Analytical	Current	No transform
0.1	0.6782711417	0.67827114	0.67828935	1.301324259	1.3013243	1.3009209	4.608623005	4.6086230	4.6000426
0.01	0.7213302408	0.72133024	0.71618918	2.450973403	2.4509734	1.9762292	49.60717163	49.607172	16.893603
0.001	0.7258107954	0.72581080	0.71705541	3.602249449	3.6022494	2.0027182	499.607157	499.60716	17.633306
0.0001	0.7262606009	0.72626060	0.71705550	4.753541831	4.7535418	2.0029931	4999.607157	4999.6072	17.641090
0.00001	0.726305599	0.72630560	0.71705550	5.904834376	5.9048344	2.0029959	49999.60716	49999.607	17.641168
0.000001	0.726310099	0.72631010	0.71705550	7.056126922	7.0561269	2.0029959	499999.6072	499999.61	17.641169

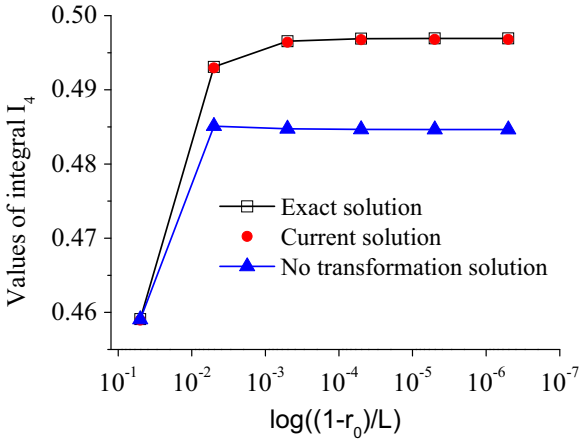

Fig. 11. The results of I_4 when r_0 varies from 0.9 to 0.999999.

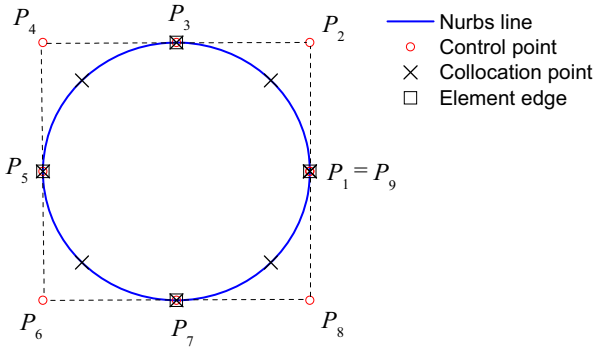

Fig. 12. The isogeometric model of circular plate.

gradually close to the boundary (Fig. 15(b)–(e)), the results obtained by the conventional IGBEM become less satisfactory or even invalid. In contrast, the results from the present method are well consistent with the exact solutions as d/L varies from 6.3661977×10^{-2} to $6.3661977 \times 10^{-10}$.

5.6. Temperature distribution in L-shaped model

An L-shaped model is here considered as shown in Fig. 16. The temperature distribution T in the boundary is the function that satisfies boundary conditions and the Laplace equation, i.e.,

$$\frac{\partial^2 T}{\partial x^2} + \frac{\partial^2 T}{\partial y^2} = 0 \text{ in } \Omega \tag{46}$$

Fig. 16 presents the model geometry defined by quadratic NURBS curve. The model can be practically reduced to a small number of NURBS control points. These points, for quadratic segments, are the corner and middle points, i.e.$P_1, P_2, \ldots, P_{12}$. To give an exact definition of

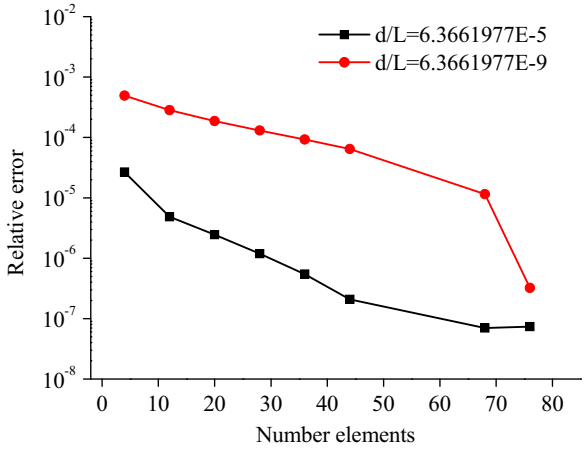

Fig. 13. Convergence curve at computed point $((r - r_0)\cos(\pi/4),\ (r - r_0)\sin(\pi/4))$.

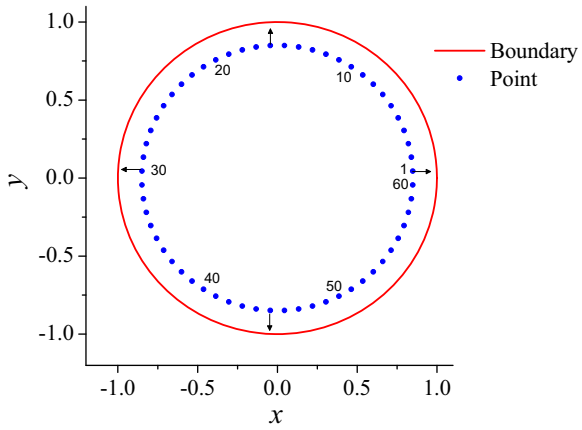

Fig. 14. 60 interior points along the circumferential uniform distribution.

the L-shaped domain and the boundary conditions , only 12 points are required. Hence the boundary is divided into 6 quadratic elements.

Table 9 and Fig. 17 show the results of temperature when the computed points are gradually close to the boundary along the line $y = 0.5$. From Table 9, it can be observed that the results obtained by both the conventional IGBEM and present method are satisfactory when $d/L \geq 0.05$. As the interior point further approaches the outer boundary, the results obtained by the conventional IGBEM are totally invalid. On the other hand, the present method can obtain accurate results even when the distance between the interior point and the outer boundary is as small as 5×10^{-8}. The same conclusions can also be obtained by Fig. 17.

Table 8
Potentials u at internal points gradually close to the boundary.

d/L	r_0	r	Exact	No transformation	Present	
					Numerical	Error
0.063661977	0.9	1.0	0.1909188E+01	0.1909108E+01	0.1909273E+01	0.4421361E−04
0.0063661977	0.99	1.0	0.2100107E+01	0.1515422E+01	0.2100174E+01	0.3173778E−04
0.00063661977	0.999	1.0	0.2119199E+01	0.1096366E+01	0.2119264E+01	0.3058104E−04
0.000063661977	0.9999	1.0	0.2121108E+01	0.1050690E+01	0.2121173E+01	0.3068230E−04
0.0000063661977	0.99999	1.0	0.2121299E+01	0.1046118E+01	0.2121361E+01	0.2925180E−04
0.00000063661977	0.999999	1.0	0.2121318E+01	0.1045661E+01	0.2121371E+01	0.2505602E−04
0.000000063661977	0.9999999	1.0	0.2121320E+01	0.1045615E+01	0.2121399E+01	0.3729100E−04
0.0000000063661977	0.99999999	1.0	0.2121320E+01	0.1045611E+01	0.2121484E+01	0.7712208E−04

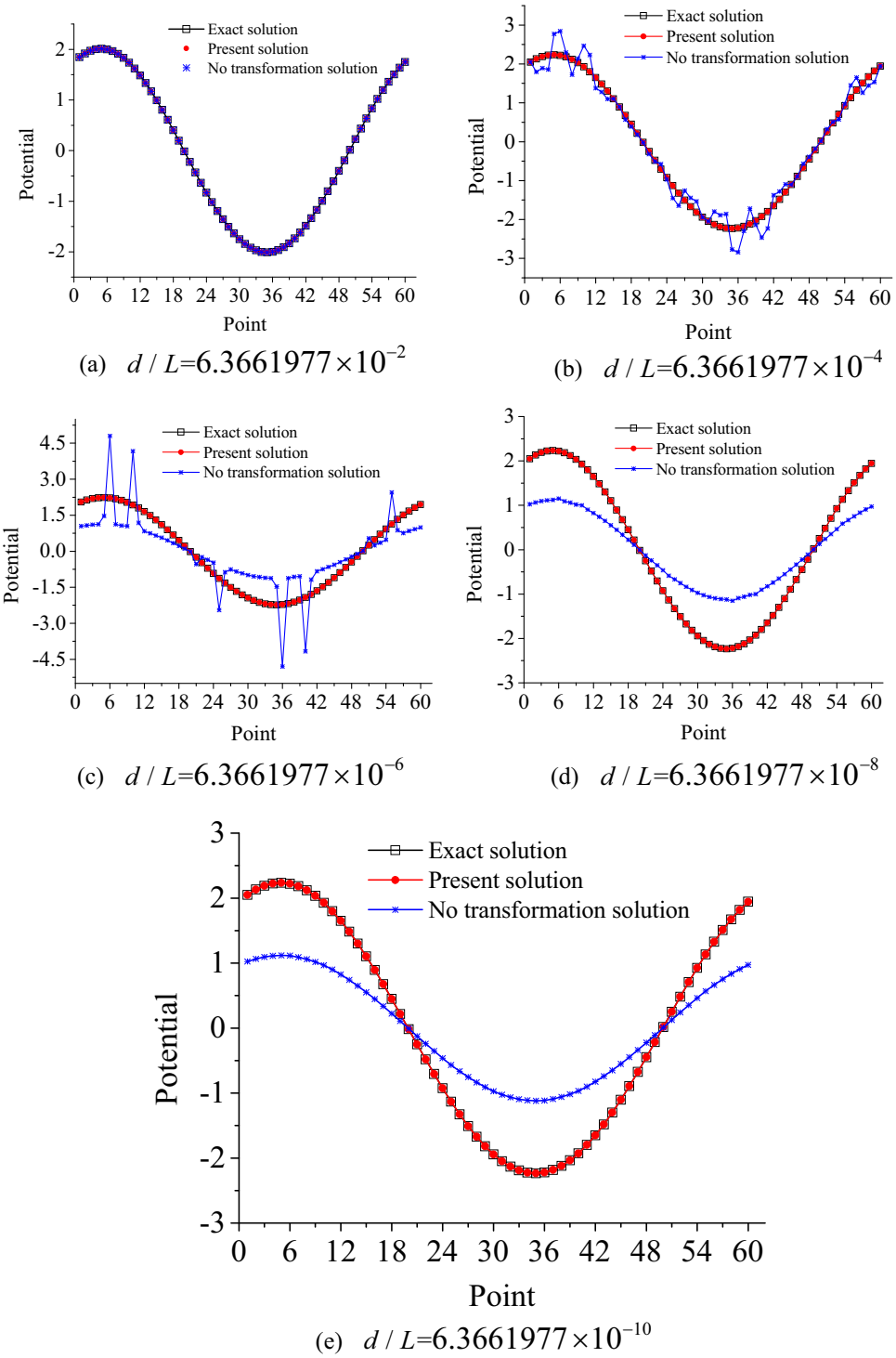

Fig. 15. The results of potential u at 60 points as the distance varies from 6.3661977×10^{-2} to 6.3661977×10^{-10}. (a) $d/L = 6.3661977\times10^{-2}$. (b) $d/L = 6.3661977\times10^{-4}$. (c) $d/L = 6.3661977\times10^{-6}$. (d) $d/L = 6.3661977\times10^{-8}$. (e) $d/L = 6.3661977\times10^{-10}$.

5.7. A model with complicated geometry

In order to show the advantages of the present method, a model built by the Rhinoceros is solved here. The geometry and computed points are shown in Fig. 18. In numerical implementation , the element is also represented as a quadratic NURBS curve with the following knot sequence

U = {0, 0, 0, 1, 1, 2, 2, 3, 3, 4, 4, 5, 5, 6, 6, 7, 7, 8, 8, 9, 9, 10, 10, 11 , 11, 12, 12, 13, 13, 14, 14,15, 15, 16, 16, 17, 17, 18, 18, 19, 19, 20, 20, 21, 21, 22, 22, 23, 23, 24, 24 , 24}.

and the control points and weights are given in Appendix B. The potential on the boundary is given as $u = x - 5$.

Numerical results of the computed points A and B are shown in Fig. 19(a) and (b), respectively. These points are located along the radius of the circle arc and gradually close to the boundary of the

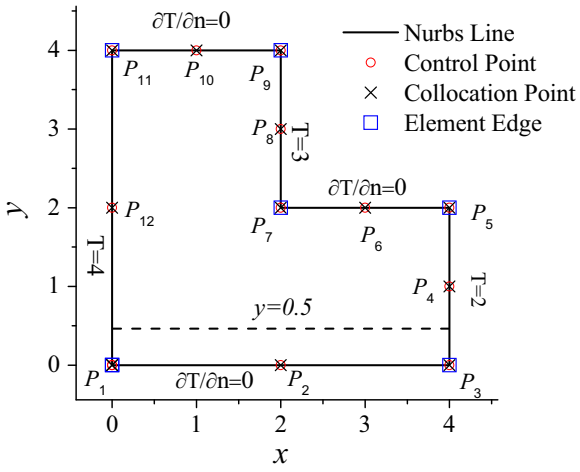

Fig. 16. The isogeometric L-shaped model.

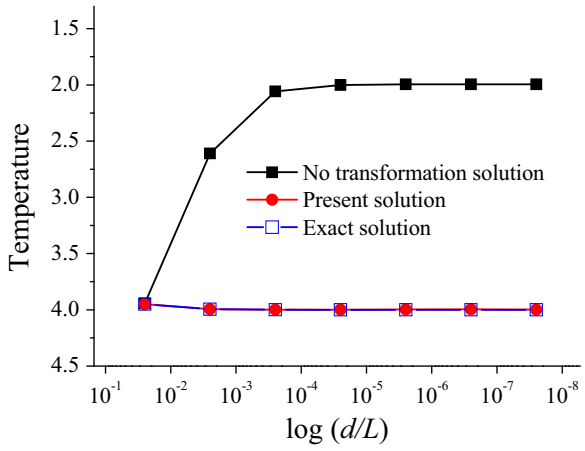

Fig. 17. The temperatures at the points being gradually close to the left boundary alone

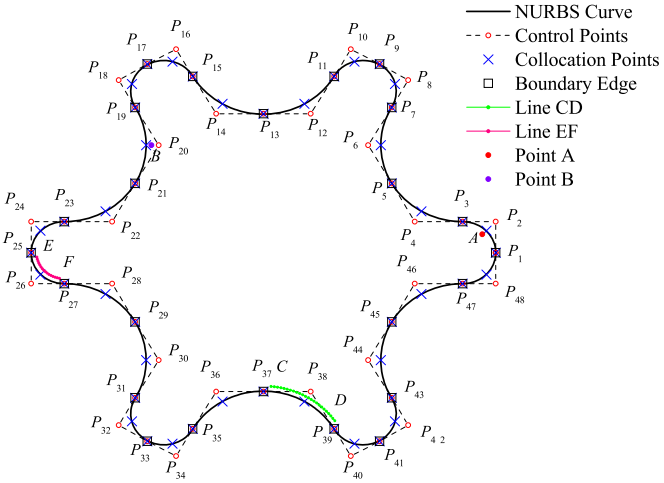

Fig. 18. The isogeometric model.

model. From Fig. 19, we can observe that the results obtained by the conventional IGBEM become invalid with the computed point is close to the boundary. While the results from the present method are well consistent with the exact solutions even when the distance between the interior point and the boundary is very small.

Fig. 20 plots the convergent curve of the potential at point A when the distance d/L from point A to the boundary is fixed as 4×10^{-6}, which shows that the convergence rate of the present method is fast. Furthermore, the present method is also stable with the increasing of the number of boundary element. Fig. 18 also gives two computed points sets, i.e. the set S_1 along the line CD and S_2 along the line EF. S_1 includes 24 computed points which are uniformly distributed along the internal curve as follows

$$x = x_1 + (R_1 + d)cos\theta, \quad y = y_1 + (R_1 + d)\sin\theta$$

where

$(x_1, y_1) = (0, -17.3205081)$, $R_1 = 6.16025406$, $d = 10^{-5}$ $(d/L = 1.6233097 \times 10^{-6})$ and $\theta \in [\frac{7\pi}{36}, \frac{17\pi}{36}]$.

And the set S_2 includes 16 computed points which are uniformly distributed along the internal curve as follows

$$x = x_2 + (R_2 + d)cos\theta, \quad y = y_2 + (R_2 + d)\sin\theta$$

where $(x_2, y_2) = (-15, 0)$, $R_2 = 2.5$, $d = 10^{-5}$ $(d/L = 4 \times 10^{-6})$, and $\theta \in [-\frac{5\pi}{9}, -\frac{17\pi}{18}]$. Fig. 21(a) and (b) show the numerical and exact results of the potential u on S_1 and S_2, respectively. It can be seen that the numerical results are excellently consistent with the exact solutions. However, the results obtained by the conventional IGBEM obviously deviate from the exact solutions.

6. Conclusions

In this paper, a general scheme is proposed to calculate the nearly singular integrals appearing in 2D/3D potential problems by using the IGBEM. The distance function is first formed when the NURBS is adopted for modeling the boundary geometry, then a nonlinear transformation, based on the exponential functions, is developed to remove or damp out the near singularities of integrands for considered integrals before applying the standard Gaussian quadrature to numerical integration. The effectiveness and accuracy of the present method have been verified through several examples. The promising results from numerical examples show that the present method is effective, stable and competitive for solving boundary layer problems of the IGBEM. In addition, some attractive features are exhibited as follow:

(1) The present work highlights the power of the IGBEM. Compared with the conventional boundary element method, the main benefit of the IGBEM is that the geometry of the problem is preserved exactly with small number of boundary elements. In contrast, for the conventional BEM large number of boundary element is needed to approximate the boundary geometry. Thus the physical quantities of points very

Table 9
The temperatures at the points being gradually close to the right boundary along the line $y = 0.5$ (the integration span L=2).

x	y	d/L	Exact	No transformation	Present	Error
0.390E+01	0.500E+00	0.05	0.2050000E+01	0.2050055E+01	0.2050001E+01	4.934012E−07
0.399E+01	0.500E+00	0.005	0.2005000E+01	0.1738219E+01	0.2005001E+01	5.588477E−07
0.3999E+01	0.500E+00	0.0005	0.2000500E+01	0.1095032E+01	0.2000501E+01	4.593563E−07
0.39999E+01	0.500E+00	0.00005	0.2000050E+01	0.1011174E+01	0.2000048E+01	1.158754E−06
0. 399999E+01	0.500E+00	0.000005	0.2000005E+01	0.1002763E+01	0.2000078E+01	3.657504E−05
0. 3999999E+01	0.500E+00	0.0000005	0.2000001E+01	0.1001922E+01	0.2000132E+01	6.551105E−05
0. 39999999E+01	0.500E+00	0.00000005	0.2000000E+01	0.1001838E+01	0.1999828E+01	8.616501E−05

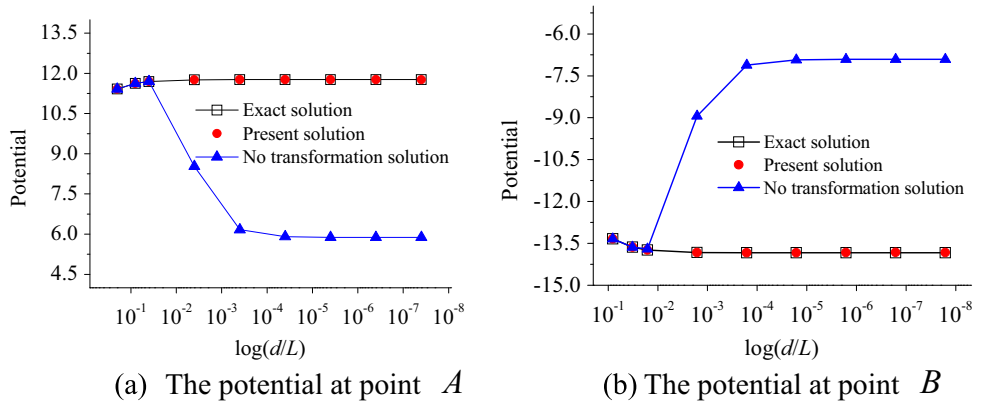

Fig. 19. The potentials at points A(integration span L=2.5) and B(integration span L=6.160254). (a) The potential at point A. (b) The potential at point B.

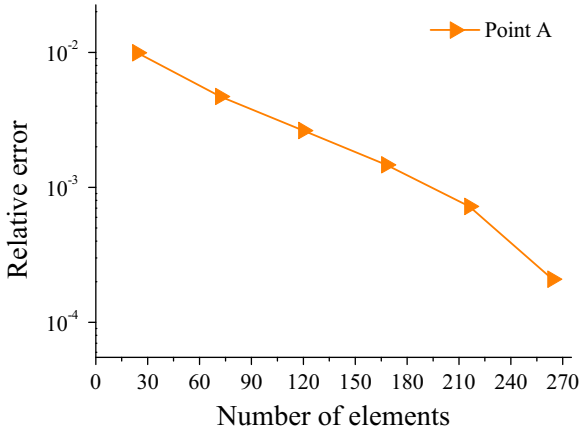

Fig. 20. Convergence curve of potential at point A.

close to the real boundary can be obtained by the IGBEM with small number of boundary elements. However, when the computed points are very close to the real boundary of the model, the nearly singular integrals appear, which covers up the advantage of the IGBEM. The present method can successfully solve the boundary layer problems of the IGBEM which highlights the advantage of the IGBEM.

(2) The present work expands the application range of the IGBEM. Due to the existence of the nearly singular integrals, it is always a challenging task to solve thin-body and coating structure problems. The present method removes the near singularities of integrands for the IGBEM, which expands the application range of the IGBEM, such as thin-body, coating structure, sensitivity analyses and contact problems.

Acknowledgements

The research is supported by the National Natural Science Foundation of China (11132011,11272054,11672038).

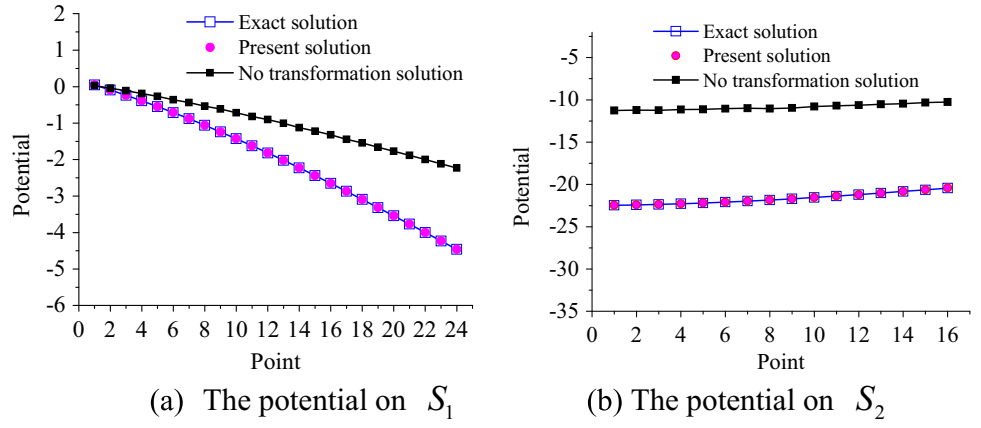

Fig. 21. The potentials on S_1 and S_2. (a) The potential on S_1. (b) The potential on S_2.

Appendix A

The detailed forms of $g_4(\xi),\ldots,g_8(\xi)$ are given as follows.
For $n = 4, \psi = \xi - \xi_p$

$$g_4(\xi) = (\mathbf{x}(\xi_p) - \mathbf{y})(\mathbf{x}^{(2)} + \tfrac{2}{3!}\psi\mathbf{x}^{(3)} + \tfrac{2}{4!}\psi^2\mathbf{x}^{(4)}) + (\mathbf{x}')^2 + \psi\mathbf{x}'\mathbf{x}^{(2)} + \tfrac{2}{3!}\psi^2\mathbf{x}'\mathbf{x}^{(3)} + \tfrac{2}{4!}\psi^3\mathbf{x}'\mathbf{x}^{(4)} + \tfrac{1}{2!2!}\psi^2(\mathbf{x}^{(2)})^2 + \tfrac{2}{2!3!}\psi^3\mathbf{x}^{(2)}\mathbf{x}^{(3)} + \tfrac{2}{2!4!}\psi^4\mathbf{x}^{(2)}\mathbf{x}^{(4)} + \tfrac{1}{3!3!}\psi^4(\mathbf{x}^{(3)})^2 + \tfrac{2}{3!4!}\psi^5\mathbf{x}^{(3)}\mathbf{x}^{(4)} + \tfrac{1}{4!4!}\psi^6(\mathbf{x}^{(4)})^2$$

For $n = 5$, $\psi = \xi - \xi_p$

$$g_5(\xi) = (\mathbf{x}(\xi_p) - \mathbf{y})(\mathbf{x}^{(2)} + \tfrac{2}{3!}\psi\mathbf{x}^{(3)} + \tfrac{2}{4!}\psi^2\mathbf{x}^{(4)} + \tfrac{2}{5!}\psi^3\mathbf{x}^{(5)}) + (\mathbf{x}')^2 + \psi\mathbf{x}^{(1)}\mathbf{x}^{(2)} + \tfrac{2}{3!}\psi^2\mathbf{x}^{(1)}\mathbf{x}^{(3)} + \tfrac{2}{4!}\psi^3\mathbf{x}^{(1)}\mathbf{x}^{(4)} + \tfrac{2}{5!}\psi^4\mathbf{x}^{(1)}\mathbf{x}^{(5)} + (\tfrac{1}{2!})^2\psi^2(\mathbf{x}^{(2)})^2 + \tfrac{2}{2!3!}\psi^3\mathbf{x}^{(2)}\mathbf{x}^{(3)} + \tfrac{2}{2!4!}\psi^4\mathbf{x}^{(2)}\mathbf{x}^{(4)} + \tfrac{2}{2!5!}\psi^5\mathbf{x}^{(2)}\mathbf{x}^{(5)} + (\tfrac{1}{3!})^2\psi^4(\mathbf{x}^{(3)})^2 + \tfrac{2}{3!4!}\psi^5\mathbf{x}^{(3)}\mathbf{x}^{(4)} + \tfrac{2}{3!5!}\psi^6\mathbf{x}^{(3)}\mathbf{x}^{(5)} + (\tfrac{1}{4!})^2\psi^6(\mathbf{x}^{(4)})^2 + \tfrac{2}{4!5!}\psi^7\mathbf{x}^{(4)}\mathbf{x}^{(5)} + (\tfrac{1}{5!})^2\psi^8(\mathbf{x}^{(5)})^2$$

For $n = 6$, $\psi = \xi - \xi_p$

$$g_6(\xi) = (\mathbf{x}(\xi_p) - \mathbf{y})(\mathbf{x}^{(2)} + \tfrac{2}{3!}\psi\mathbf{x}^{(3)} + \tfrac{2}{4!}\psi^2\mathbf{x}^{(4)} + \tfrac{2}{5!}\psi^3\mathbf{x}^{(5)} + \tfrac{2}{6!}\psi^4\mathbf{x}^{(6)}) + (\mathbf{x}')^2 + \psi\mathbf{x}^{(1)}\mathbf{x}^{(2)} + \tfrac{2}{3!}\psi^2\mathbf{x}^{(1)}\mathbf{x}^{(3)} + \tfrac{2}{4!}\psi^3\mathbf{x}^{(1)}\mathbf{x}^{(4)} + \tfrac{2}{5!}\psi^4\mathbf{x}^{(1)}\mathbf{x}^{(5)} + \tfrac{2}{6!}\psi^5\mathbf{x}^{(1)}\mathbf{x}^{(6)} + (\tfrac{1}{2!})^2\psi^2(\mathbf{x}^{(2)})^2 + \tfrac{2}{2!3!}\psi^3\mathbf{x}^{(2)}\mathbf{x}^{(3)} + \tfrac{2}{2!4!}\psi^4\mathbf{x}^{(2)}\mathbf{x}^{(4)} + \tfrac{2}{2!5!}\psi^5\mathbf{x}^{(2)}\mathbf{x}^{(5)} + \tfrac{2}{2!6!}\psi^6\mathbf{x}^{(2)}\mathbf{x}^{(6)} + (\tfrac{1}{3!})^2\psi^4(\mathbf{x}^{(3)})^2 + \tfrac{2}{3!4!}\psi^5\mathbf{x}^{(3)}\mathbf{x}^{(4)} + \tfrac{2}{3!5!}\psi^6\mathbf{x}^{(3)}\mathbf{x}^{(5)} + \tfrac{2}{3!6!}\psi^7\mathbf{x}^{(3)}\mathbf{x}^{(6)} + (\tfrac{1}{4!})^2\psi^6(\mathbf{x}^{(4)})^2 + \tfrac{2}{4!5!}\psi^7\mathbf{x}^{(4)}\mathbf{x}^{(5)} + \tfrac{2}{4!6!}\psi^8\mathbf{x}^{(4)}\mathbf{x}^{(6)} + (\tfrac{1}{5!})^2\psi^8(\mathbf{x}^{(5)})^2 + \tfrac{2}{5!6!}\psi^9\mathbf{x}^{(5)}\mathbf{x}^{(6)} + (\tfrac{1}{6!})^2\psi^{10}(\mathbf{x}^{(6)})^2$$

For $n = 7$, $\psi = \xi - \xi_p$

$$g_7(\xi) = (\mathbf{x}(\xi_p) - \mathbf{y})(\mathbf{x}^{(2)} + \tfrac{2}{3!}\psi\mathbf{x}^{(3)} + \tfrac{2}{4!}\psi^2\mathbf{x}^{(4)} + \tfrac{2}{5!}\psi^3\mathbf{x}^{(5)} + \tfrac{2}{6!}\psi^4\mathbf{x}^{(6)} + \tfrac{2}{7!}\psi^5\mathbf{x}^{(7)}) + (\mathbf{x}')^2 + \psi\mathbf{x}^{(1)}\mathbf{x}^{(2)} + \tfrac{2}{3!}\psi^2\mathbf{x}^{(1)}\mathbf{x}^{(3)} + \tfrac{2}{4!}\psi^3\mathbf{x}^{(1)}\mathbf{x}^{(4)} + \tfrac{2}{5!}\psi^4\mathbf{x}^{(1)}\mathbf{x}^{(5)} + \tfrac{2}{6!}\psi^5\mathbf{x}^{(1)}\mathbf{x}^{(6)} + \tfrac{2}{7!}\psi^6\mathbf{x}^{(1)}\mathbf{x}^{(7)} + (\tfrac{1}{2!})^2\psi^2(\mathbf{x}^{(2)})^2 + \tfrac{2}{2!3!}\psi^3\mathbf{x}^{(2)}\mathbf{x}^{(3)} + \tfrac{2}{2!4!}\psi^4\mathbf{x}^{(2)}\mathbf{x}^{(4)} + \tfrac{2}{2!5!}\psi^5\mathbf{x}^{(2)}\mathbf{x}^{(5)} + \tfrac{2}{2!6!}\psi^6\mathbf{x}^{(2)}\mathbf{x}^{(6)} + \tfrac{2}{2!7!}\psi^7\mathbf{x}^{(2)}\mathbf{x}^{(7)} + (\tfrac{1}{3!})^2\psi^4(\mathbf{x}^{(3)})^2 + \tfrac{2}{3!4!}\psi^5\mathbf{x}^{(3)}\mathbf{x}^{(4)} + \tfrac{2}{3!5!}\psi^6\mathbf{x}^{(3)}\mathbf{x}^{(5)} + \tfrac{2}{3!6!}\psi^7\mathbf{x}^{(3)}\mathbf{x}^{(6)} + \tfrac{2}{3!7!}\psi^8\mathbf{x}^{(3)}\mathbf{x}^{(7)} + (\tfrac{1}{4!})^2\psi^6(\mathbf{x}^{(4)})^2 + \tfrac{2}{4!5!}\psi^7\mathbf{x}^{(4)}\mathbf{x}^{(5)} + \tfrac{2}{4!6!}\psi^8\mathbf{x}^{(4)}\mathbf{x}^{(6)} + \tfrac{2}{4!7!}\psi^9\mathbf{x}^{(4)}\mathbf{x}^{(7)} + (\tfrac{1}{5!})^2\psi^8(\mathbf{x}^{(5)})^2 + \tfrac{2}{5!6!}\psi^9\mathbf{x}^{(5)}\mathbf{x}^{(6)} + \tfrac{2}{5!7!}\psi^{10}\mathbf{x}^{(5)}\mathbf{x}^{(7)} + (\tfrac{1}{6!})^2\psi^{10}(\mathbf{x}^{(6)})^2 + \tfrac{2}{6!7!}\psi^{11}\mathbf{x}^{(6)}\mathbf{x}^{(7)} + (\tfrac{1}{7!})^2\psi^{12}(\mathbf{x}^{(7)})^2$$

For $n = 8$, $\psi = \xi - \xi_p$

$$g_8(\xi) = (\mathbf{x}(\xi_p) - \mathbf{y})(\mathbf{x}^{(2)} + \tfrac{2}{3!}\psi\mathbf{x}^{(3)} + \tfrac{2}{4!}\psi^2\mathbf{x}^{(4)} + \tfrac{2}{5!}\psi^3\mathbf{x}^{(5)} + \tfrac{2}{6!}\psi^4\mathbf{x}^{(6)} + \tfrac{2}{7!}\psi^5\mathbf{x}^{(7)} + \tfrac{2}{8!}\psi^6\mathbf{x}^{(8)}) + (\mathbf{x}')^2 + \psi\mathbf{x}^{(1)}\mathbf{x}^{(2)} + \tfrac{2}{3!}\psi^2\mathbf{x}^{(1)}\mathbf{x}^{(3)} + \tfrac{2}{4!}\psi^3\mathbf{x}^{(1)}\mathbf{x}^{(4)} + \tfrac{2}{5!}\psi^4\mathbf{x}^{(1)}\mathbf{x}^{(5)} + \tfrac{2}{6!}\psi^5\mathbf{x}^{(1)}\mathbf{x}^{(6)} + \tfrac{2}{7!}\psi^6\mathbf{x}^{(1)}\mathbf{x}^{(7)} + \tfrac{2}{8!}\psi^7\mathbf{x}^{(1)}\mathbf{x}^{(8)} + (\tfrac{1}{2!})^2\psi^2(\mathbf{x}^{(2)})^2 + \tfrac{2}{2!3!}\psi^3\mathbf{x}^{(2)}\mathbf{x}^{(3)} + \tfrac{2}{2!4!}\psi^4\mathbf{x}^{(2)}\mathbf{x}^{(4)} + \tfrac{2}{2!5!}\psi^5\mathbf{x}^{(2)}\mathbf{x}^{(5)} + \tfrac{2}{2!6!}\psi^6\mathbf{x}^{(2)}\mathbf{x}^{(6)} + \tfrac{2}{2!7!}\psi^7\mathbf{x}^{(2)}\mathbf{x}^{(7)} + \tfrac{2}{2!8!}\psi^8\mathbf{x}^{(2)}\mathbf{x}^{(8)} + (\tfrac{1}{3!})^2\psi^4(\mathbf{x}^{(3)})^2 + \tfrac{2}{3!4!}\psi^5\mathbf{x}^{(3)}\mathbf{x}^{(4)} + \tfrac{2}{3!5!}\psi^6\mathbf{x}^{(3)}\mathbf{x}^{(5)} + \tfrac{2}{3!6!}\psi^7\mathbf{x}^{(3)}\mathbf{x}^{(6)} + \tfrac{2}{3!7!}\psi^8\mathbf{x}^{(3)}\mathbf{x}^{(7)} + \tfrac{2}{3!8!}\psi^9\mathbf{x}^{(3)}\mathbf{x}^{(8)} + (\tfrac{1}{4!})^2\psi^6(\mathbf{x}^{(4)})^2 + \tfrac{2}{4!5!}\psi^7\mathbf{x}^{(4)}\mathbf{x}^{(5)} + \tfrac{2}{4!6!}\psi^8\mathbf{x}^{(4)}\mathbf{x}^{(6)} + \tfrac{2}{4!7!}\psi^9\mathbf{x}^{(4)}\mathbf{x}^{(7)} + \tfrac{2}{4!8!}\psi^{10}\mathbf{x}^{(4)}\mathbf{x}^{(8)} + (\tfrac{1}{5!})^2\psi^8(\mathbf{x}^{(5)})^2 + \tfrac{2}{5!6!}\psi^9\mathbf{x}^{(5)}\mathbf{x}^{(6)} + \tfrac{2}{5!7!}\psi^{10}\mathbf{x}^{(5)}\mathbf{x}^{(7)} + \tfrac{2}{5!8!}\psi^{11}\mathbf{x}^{(5)}\mathbf{x}^{(8)} + (\tfrac{1}{6!})^2\psi^{10}(\mathbf{x}^{(6)})^2 + \tfrac{2}{6!7!}\psi^{11}\mathbf{x}^{(6)}\mathbf{x}^{(7)} + \tfrac{2}{6!8!}\psi^{12}\mathbf{x}^{(6)}\mathbf{x}^{(8)} + (\tfrac{1}{7!})^2\psi^{12}(\mathbf{x}^{(7)})^2 + \tfrac{2}{7!8!}\psi^{13}\mathbf{x}^{(7)}\mathbf{x}^{(8)} + (\tfrac{1}{8!})^2\psi^{14}(\mathbf{x}^{(8)})^2$$

Appendix B

The control points and weights of the considered model are listed in Table 10.

Table 10
The control points and weights of the considered model in Fig. 18.

Control points	Coordinates	Weights
P_1	(17.5,0.0)	1.0
P_2	(17.5,2.5)	$\sqrt{2}/2\sqrt{2}/2$
P_3	(15.0,2.5)	1.0
P_4	(11.4433757,2.5)	$\sqrt{3}/2$
P_5	(9.6650635,5.5801270)	1.0
P_6	(7.8867513,8.6602540)	$\sqrt{3}/2$

(continued on next page)

Table 10 *(continued)*

Control points	Coordinates	Weights
P_7	(9.6650635,11.7403811)	1.0
P_8	(10.9150635,13.9054446)	$\sqrt{2}/2$
P_9	(8.7500000,15.1554446)	1.0
P_{10}	(6.5849365,16.4054446)	$\sqrt{2}/2$
P_{11}	(5.3349365,14.2403811)	1.0
P_{12}	(3.5566243,11.1602540)	$\sqrt{3}/2$
P_{13}	(0.0,11.1602540)	1.0
P_{14}	(−3.5566243,11.1602540)	$\sqrt{3}/2$
P_{15}	(−5.3349365,14.2403811)	1.0
P_{16}	(−6.5849365,16.4054446)	$\sqrt{2}/2$
P_{17}	(−8.7500000,15.1554446)	1.0
P_{18}	(−10.9150635,13.9054446)	$\sqrt{2}/2$
P_{19}	(−9.6650635,11.7403811)	1.0
P_{20}	(−7.8867513,8.6602540)	$\sqrt{3}/2$
P_{21}	(−9.6650635,5.5801270)	1.0
P_{22}	(−11.4433757,2.5)	$\sqrt{3}/2$
P_{23}	(−15.0,2.5)	1.0
P_{24}	(−17.5,2.5)	$\sqrt{2}/2$
P_{25}	(−17.5,0.0)	1.0
P_{26}	(−17.5,−2.5)	$\sqrt{2}/2$
P_{27}	(−15.0,−2.5)	1.0
P_{28}	(−11.4433757,−2.5)	$\sqrt{3}/2$
P_{29}	(−9.6650635,−5.5801270)	1.0
P_{30}	(−7.8867513,−8.6602540)	$\sqrt{3}/2$
P_{31}	(−9.6650635,−11.7403811)	1.0
P_{32}	(−10.9150635,−13.9054446)	$\sqrt{2}/2$
P_{33}	(−8.75,−15.1554446)	1.0
P_{34}	(−6.5849365,−16.4054446)	$\sqrt{2}/2$
P_{35}	(−5.3349365,−14.2403811)	1.0
P_{36}	(−3.5566243,−11.1602540)	$\sqrt{3}/2$
P_{37}	(0.0,−11.1602540)	1.0
P_{38}	(3.5566243,−11.1602540)	$\sqrt{3}/2$
P_{39}	(5.3349365,−14.2403811)	1.0
P_{40}	(6.5849365,−16.4054446)	$\sqrt{2}/2$
P_{41}	(8.75,−15.1554446)	1.0
P_{42}	(10.9150635,−13.9054446)	$\sqrt{2}/2$
P_{43}	(9.6650635,−11.7403811)	1.0
P_{44}	(7.8867513,−8.6602540)	$\sqrt{3}/2$
P_{45}	(9.6650635,−5.5801270)	1.0
P_{46}	(11.4433757,−2.5)	$\sqrt{3}/2$
P_{47}	(15.0,−2.5)	1.0
P_{48}	(17.5,−2.5)	$\sqrt{2}/2$
P_{49}	(17.5,0.0)	1.0

References

[1] Hughes TJR, Cottrell JA, Bazilevs Y. Isogeometric analysis: CAD, finite elements, NURBS, exact geometry and mesh refinement. Comput Methods Appl Mech Eng 2005;194:4135–95.

[2] Cottrell JA, Hughes TJR, Reali A. Studies of refinement and continuity in isogeometric analysis. Comput Methods Appl Mech Eng 2007;196:4160–83.

[3] Cottrell JA, Reali A, Bazilevs Y, Hughes TJR. Isogeometric analysis of structural vibrations. Comput Methods Appl Mech Eng 2006;195:5257–96.

[4] Bazilevs Y, Calo VM, Zhang Y, Hughes TJR. Isogeometric fluid–structure interaction analysis with applications to arterial blood flow. Comput Methods Appl Mech Eng 2006;38:310–22.

[5] Bazilevs Y, Beirao de Veiga L, Cottrell JA, Hughes TJR, Sangalli G. Isogeometric analysis: approximation, stability and error estimates for h-refined meshes, math models. Methods Appl Sci 2006;16:1031–90.

[6] Zhang Y, Bazilevs Y, Goswami S, Bajaj C, Hughes TJR. Patient-specific vascular NURBS modeling for isogeometric analysis of blood flow. Comput Methods Appl Mech Eng 2007;196:2943–59.

[7] Simpson RN, Bordas SPA, Trevelyan J, Rabczuk T. A two-dimensional isogeometric boundary element method for elastostatic analysis. Comput Methods Appl Mech Eng 209 2012;212:87–100.

[8] Gu JL, Zhang JM, Li GY. Isogeometric analysis in BIE for 3-D potential problem. Eng Anal Bound Elem 2012;36:858–65.

[9] Takahashi T, Matsumoto T. An application of fast multipole method to isogeometric boundary element method for Laplace equation in two dimensions. Eng Anal Bound Elem 2012;36:1766–75.

[10] Peake MJ, Trevelyan J, Coates G. Extended isogeometric boundary element method (XIBEM) for two-dimensional Helmholtz problems. Comput Methods Appl Mech Eng 2013;259:93–102.

[11] Belibassakis KA, Gerostathis ThP, Kostas KV, Politis CG, Kaklis PD, Ginnis AI, Feurer C. A BEM-isogeometric method for the ship wave-resistance problem. Ocean Eng 2013;60:53–67.

[12] Ginnisa AI, Kostasb KV, Politisb CG, Kaklisa PD, Belibassakisa KA, Gerostathisb ThP, Scottd MA, Hughes TJR. Isogeometric boundary-element analysis for the wave-resistance problem using T-splines. Comput Methods Appl Mech Eng 2014;279:425–39.

[13] Simpson RN, Scott MA, Taus M, Thomas DC, Lian H. Acoustic isogeometric boundary element analysis. Comput Methods Appl Mech Eng 2014;269:265–90.

[14] Peake MJ, Trevelyan J, Coates G. Extended isogeometric boundary element method (XIBEM) for three-dimensional medium-wave acoustic scattering problems. Comput Methods Appl Mech Eng 2015;284:762–80.

[15] Kostas KV, Ginnis AI, Politis CG, Kaklis PD. Ship-hull shape optimization with a T-spline based BEM–isogeometric solver. Comput Methods Appl Mech Eng 2015;284:611–22.

[16] Wang YJ, Benson DJ. Multi-patch nonsingular isogeometric boundary element analysis in 3D. Comput Methods Appl Mech Eng 2015;293:71–91.

[17] Feischl M, Gantner G, Praetorius D. Reliable and efficient a posteriori error estimation for adaptive IGA boundary element methods for weakly-singular integral equations. Comput Methods Appl Mech Eng 2015;290:362–86.

[18] Simpson RN, Bordas SPA, Lian H, Trevelyan J. An isogeometric boundary element method for elastostatic analysis: 2D implementation aspects. Comput Struct

2013;118:2–12.
[19] Bai Y, Dong CY, Liu ZY. Effective elastic properties and stress states of doubly periodic array of inclusions with complex shapes by isogeometric boundary element method. Compos Struct 2015;128:54–69.
[20] Gu JL, Zhang JM, Chen LF, Cai ZH. An isogeometric BEM using PB-spline for 3-D linear elasticity problem. Eng Anal Bound Elem 2015;56:154–61.
[21] Nguyen BH, Tran HD, Anitescu C, Zhuang X, Rabczuk T. An isogeometric symmetric Galerkin boundary element method for two-dimensional crack problems. Comput Methods Appl Mech Eng 2016;306:252–75.
[22] Farin G, Hoschek J, Kim M-S, editors. Handbook of Computer Aided Geometric Design. Amsterdam: Elsevier; 2002.
[23] Liu YJ. Analysis of shell-like structures by the boundary element method based on 3-D elasticity: formulation and verification. Int J Numer Methods Eng 1998;41:541–58.
[24] Zhang YM, Gu Y, Chen JT. Boundary element analysis of 2D thin walled structures with high-order geometry elements using transformation. Eng Anal Bound Elem 2011;35(3):581–6.
[25] Aliabadi MH, Martin D. Boundary element hyper-singular formulation for elasto-plastic contact problems. Int J Numer Methods Eng 2000;48:995–1014.
[26] Zhang D, Rizzo FJ, Rudolphi YJ. Stress intensity sensitivities via hypersingular boundary element integral equations. Comput Mech 1999;23:389–96.
[27] Dirgantara T, Aliabadi MH. Crack growth analysis of plates loaded by bending and tension using dual boundary element method. Int J Fract 2000;105:27–74.
[28] Okada H, Rajiyah H, Atluri SN. Non-hyper-singular integral rep- resentations for velocity (displacement) gradients in elastic/plastic solids (small or finite deformations). Comput Mech 1989;4:165–75.
[29] Okada H, Rajiyah H, Atluri SN. A Full tangent stiffness field- boundary element formulation for geometric and material nonlinear problems of solid mechanics. Int J Numer Method Eng 1990;29:15–35.
[30] Sladek V, Sladek J, Tanaka M. Nonsingular BEM formulations for thin-walled structures and elastostatic crack problems. Acta Mech 1993;99:173–90.
[31] Zhang YM, Sun HC. Theoretic analysis on virtual boundary element. Chin J Comp Mech 2000;17:56–62, [in Chinese].
[32] Liu CS, Chang CW, Chang JR. A new shooting method for solving boundary layer equations in fluid mechanics. CMES: Comp Model Eng Sci 2008;32(1):1–15.
[33] Mukherjee S, Chati MK, Shi XL. Evaluation of nearly singular integrals in boundary element contour and node methods for three-dimensional linear elasticity. Int J Sol Struct 2000;37:7633–54.
[34] Gao XW, Yang K, Wang J. An adaptive element subdivision technique for evaluation of various 2D singular boundary integrals. Eng Anal Bound Elem 2008;32:692–6.
[35] Telles JCF. A self-adaptive coordinate transformation for efficient numerical evaluation of general boundary element integral. Int J Numer Methods Eng 1987;24:959–73.
[36] Earlin L. Exact Gaussian quadrature methods for near-singular integrals in the boundary element method. Eng Anal Bound Elem 1992;9:233–45.
[37] Cerrolaza M, Alarcon E. A bi-cubic transformation for the numerical evaluation of the Cauchy principal value integrals in boundary methods. Int J Numer Methods Eng 1989;28(5):987, [299].
[38] Letizia S. A new smoothing strategy for computing nearly singular integrals in 3D Galerkin BEM. J Comput Appl Math 2009;225:406–27.
[39] Ye WJ. A new transformation technique for evaluating nearly singular integrals. Comput Mech 2008;42:457–66.
[40] Sladek V, Sladek J, Tanaka M. Optimal transformations of the integration variables in computation of singular integrals in BEM. Int J Numer Methods Eng 2000;47(7):1263–83.
[41] Johnston PR. Application of sigmoidal transformations to weakly singular and near singular boundary element integrals. Int J Numer Methods Eng 1999;45(10):1333–48.
[42] Johnston BM, Johnston PR, David E. A new method for the numerical evaluation of nearly singular integrals on triangular elements in the 3D boundary element method. J Comput Appl Math 2013;245:148–61.
[43] Johnston BM, Johnston PR, David E. A sinh transformation for evaluating two-dimensional nearly singular boundary element integrals. Int J Numer Methods Eng 2007;69:1460–79.
[44] Lv JH, Miao Y, Gong WH, et al. The sinh transformation for curved elements using the general distance function. Comput Model Eng Sci 2013;93(2):113–31.
[45] Huang Q, Cruse TA. Some notes on singular integral techniques in boundary element analysis. Int J Numer Methods Eng 1993;36(15):2643–59.
[46] Ma H, Kamiya N. Distance transformation for the numerical evaluation of near singular boundary integrals with various kernels in boundary element method. Eng Anal Bound Elem 2002;26(4):329, [239].
[47] Ma H, Kamiya N. A general algorithm for the numerical evaluation of nearly singular boundary integrals of various orders for two-and three-dimensional elasticity. Comput Mech 2002;29:277–88.
[48] Zhang YM, Gu Y, Chen JT. Boundary layer effect in BEM with high order geometry elements using transformation. Comput Model Eng Sci 2009;45(3):227–47.
[49] Zhang YM, Gu Y, Chen JT. Internal stress analysis for single and multilayered coating systems using the boundary element method. Eng Anal Bound Elem 2010;35(4):708–17.
[50] Qin XY, Zhang JM, Xie GZ, et al. A general algorithm for the numerical evaluation of nearly singular integrals on 3D boundary element. J Comp Appl Math 2011;235:4174–86.
[51] Zhang YM, Qu WZ, Chen JT. BEM analysis of thin structures for thermoelastic problems. Engrg Anal Bound Elem 2013;37:441–52.
[52] Xie GZ, Zhou FL, Zhang JM, et al. New variable transformations for evaluating nearly singular integrals in 3D boundary element method. Eng Anal Bound Elem 2013;37:1169–78.
[53] Liu YJ, Zhang DM, Rizzo FJ. Nearly singular and hypersingular integrals in the boundary element method, Boundary Elements XV. In: Proceedings of the 15th International Conference on Boundary Elements, Worcester, Massachu- setts, USA; 10–12 August 1993. pp. 453–68.
[54] Luo JF, Liu YJ, Berger EJ. Analysis of two-dimensional thin structures (from micro-to nano-scales) using the boundary element method. Comput Mech 1998;22(5):404–12.
[55] Chen XL, Liu YJ. An advanced 3-D boundary element method for characterizations of composite materials. Eng Anal Bound Elem 2005;29(6):513–23.
[56] Hayami K, Matsumoto H. A numerical quadrature for nearly singular boundary element integrals. Engrg Anal Bound Elem 1994;13:143–54.
[57] lv JH, Miao Y, Zhu HP. The distance sinh transformation for the numerical evaluation of nearly singular integrals over curved surface elements. Comput Mech 2014;53:359–69.